nature medicine

TRPM2-mediated Ca^{2+} influx induces chemokine production in monocytes that aggravates inflammatory neutrophil infiltration

Shinichiro Yamamoto[1], Shunichi Shimizu[2], Shigeki Kiyonaka[1], Nobuaki Takahashi[1], Teruaki Wajima[1], Yuji Hara[1], Takaharu Negoro[3], Toshihito Hiroi[2], Yuji Kiuchi[2], Takaharu Okada[1], Shuji Kaneko[4], Ingo Lange[5], Andrea Fleig[5], Reinhold Penner[5], Miyuki Nishi[6], Hiroshi Takeshima[6] & Yasuo Mori[1]

Reactive oxygen species (ROS) induce chemokines responsible for the recruitment of inflammatory cells to sites of injury or infection. Here we show that the plasma membrane Ca^{2+}-permeable channel TRPM2 controls ROS-induced chemokine production in monocytes. In human U937 monocytes, hydrogen peroxide (H_2O_2) evokes Ca^{2+} influx through TRPM2 to activate Ca^{2+}-dependent tyrosine kinase Pyk2 and amplify Erk signaling via Ras GTPase. This elicits nuclear translocation of nuclear factor-κB essential for the production of the chemokine interleukin-8 (CXCL8). In monocytes from *Trpm2*-deficient mice, H_2O_2-induced Ca^{2+} influx and production of the macrophage inflammatory protein-2 (CXCL2), the mouse CXCL8 functional homolog, were impaired. In the dextran sulfate sodium-induced colitis inflammation model, CXCL2 expression, neutrophil infiltration and ulceration were attenuated by *Trpm2* disruption. Thus, TRPM2 Ca^{2+} influx controls the ROS-induced signaling cascade responsible for chemokine production, which aggravates inflammation. We propose functional inhibition of TRPM2 channels as a new therapeutic strategy for treating inflammatory diseases.

The biological purpose of inflammation is to bring fluids, proteins and inflammatory cells such as neutrophils and monocytes from the blood into the damaged tissues to eliminate the injuring agents and trigger the healing and repairing processes. Development of inflammatory reactions is controlled by a number of cellular and molecular components, including proinflammatory cytokines. Chemotactic cytokines, known as the chemokines, have a key role in mediating the recruitment of inflammatory cells to inflamed sites[1]. Among four subfamilies of chemokines[1], CXC chemokines such as CXCL8 and its functional homolog CXCL2 (ref. 2) are known to show potent neutrophil chemotactic activity.

At inflamed sites, neutrophils deploy a potent antimicrobial arsenal that includes proteinases, antimicrobial peptides and ROS[3]. Although ROS are extremely antimicrobial by virtue of their ability to kill microbial pathogens, in chronic inflammation, the continued production of ROS by neutrophils causes extensive tissue damage. Traditionally, this has been considered as random damage to cellular components[4]. Recently, ROS have emerged as signal transduction molecules[5]. In inflammatory cells, ROS contribute to the expression of a variety of different inflammatory cytokines, adhesion molecules and enzymes by activating redox-sensitive transcription factors such as nuclear factor-κB (NF-κB)[5].

Once monocytes adhere to endothelial cells from the bloodstream and migrate toward tissues, they differentiate into macrophages. During homeostasis, monocytes and macrophages phagocytose and remove senescent and apoptotic cells, whereas during inflammation they are the main effectors of innate immunity because of their antimicrobial activity and production of proinflammatory cytokines[6]. In human monocytes, CXCL8 production is induced by ROS, including by H_2O_2 (ref. 7) via Erk-activated NF-κB (ref. 8). It seems that increases in intracellular Ca^{2+} concentration ($[Ca^{2+}]_i$) control the production of certain cytokines, including interleukin-2 (IL-2) in T cells[9] and CXCL8 in monocytes[10]. The primary source for Ca^{2+} is probably extracellular, as reported in *Mycobacterium bovis*–induced CXCL8 production involving NF-κB (ref. 11). Despite these noteworthy indications of the regulation of CXCL8 production by ROS and Ca^{2+} influx in monocytes, the molecular entities and signaling mechanisms that connect ROS, Ca^{2+} and chemokines are not clear.

Ca^{2+} influx is mediated through plasma membrane Ca^{2+}-permeable cation channels. The *Drosophila melanogaster* transient receptor

[1]Department of Synthetic Chemistry and Biological Chemistry, Graduate School of Engineering, Kyoto University, Katsura Campus, Nishikyo-ku, Kyoto 615-8510, Japan. [2]Department of Pathophysiology and [3]Department of Medicinal Information, School of Pharmaceutical Sciences, Showa University, 1-5-8 Hatanodai, Shinagawa-ku, Tokyo 142-8555, Japan. [4]Department of Molecular Pharmacology, Graduate School of Pharmaceutical Sciences, Kyoto University, 46-29 Yoshida-Shimo-Adachi-cho, Sakyo-ku, Kyoto 606-8501, Japan. [5]Laboratory of Cell and Molecular Signaling, Center for Biomedical Research at The Queen's Medical Center and John A. Burns School of Medicine at University of Hawaii, 1301 Punchbowl Street, Honolulu, Hawaii 96813, USA. [6]Department of Biological Chemistry, Graduate School of Pharmaceutical Sciences, Kyoto University, 46-29 Yoshida-Shimo-Adachi-cho, Sakyo-ku, Kyoto 606-8501, Japan. Correspondence should be addressed to Y.M. (mori@sbchem.kyoto-u.ac.jp).

Received 14 December 2007; accepted 25 March 2008; published online 8 June 2008; doi:10.1038/nm1758

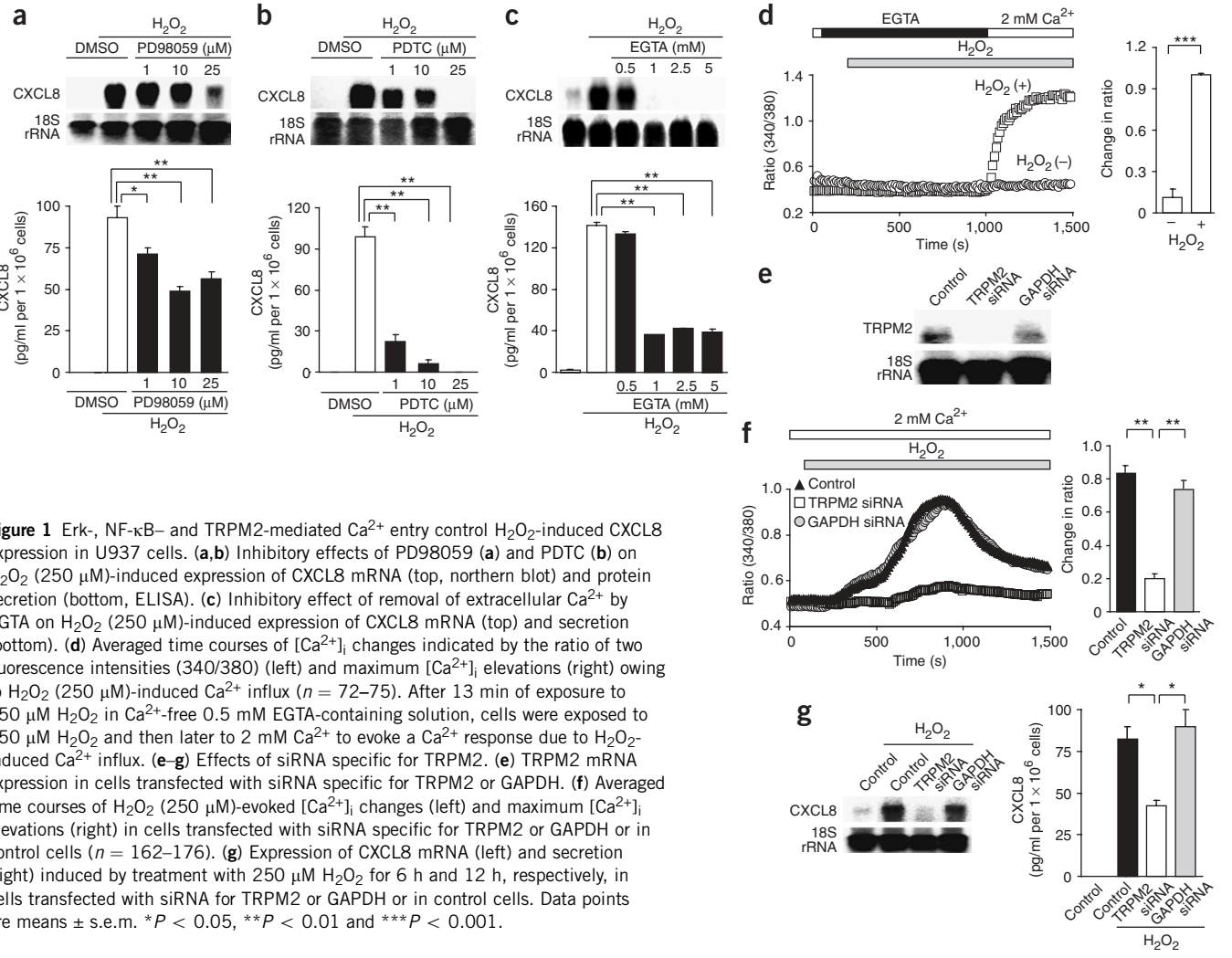

Figure 1 Erk-, NF-κB– and TRPM2-mediated Ca^{2+} entry control H_2O_2-induced CXCL8 expression in U937 cells. (**a**,**b**) Inhibitory effects of PD98059 (**a**) and PDTC (**b**) on H_2O_2 (250 μM)-induced expression of CXCL8 mRNA (top, northern blot) and protein secretion (bottom, ELISA). (**c**) Inhibitory effect of removal of extracellular Ca^{2+} by EGTA on H_2O_2 (250 μM)-induced expression of CXCL8 mRNA (top) and secretion (bottom). (**d**) Averaged time courses of $[Ca^{2+}]_i$ changes indicated by the ratio of two fluorescence intensities (340/380) (left) and maximum $[Ca^{2+}]_i$ elevations (right) owing to H_2O_2 (250 μM)-induced Ca^{2+} influx ($n = 72$–75). After 13 min of exposure to 250 μM H_2O_2 in Ca^{2+}-free 0.5 mM EGTA-containing solution, cells were exposed to 250 μM H_2O_2 and then later to 2 mM Ca^{2+} to evoke a Ca^{2+} response due to H_2O_2-induced Ca^{2+} influx. (**e**–**g**) Effects of siRNA specific for TRPM2. (**e**) TRPM2 mRNA expression in cells transfected with siRNA specific for TRPM2 or GAPDH. (**f**) Averaged time courses of H_2O_2 (250 μM)-evoked $[Ca^{2+}]_i$ changes (left) and maximum $[Ca^{2+}]_i$ elevations (right) in cells transfected with siRNA specific for TRPM2 or GAPDH or in control cells ($n = 162$–176). (**g**) Expression of CXCL8 mRNA (left) and secretion (right) induced by treatment with 250 μM H_2O_2 for 6 h and 12 h, respectively, in cells transfected with siRNA for TRPM2 or GAPDH or in control cells. Data points are means ± s.e.m. $^*P < 0.05$, $^{**}P < 0.01$ and $^{***}P < 0.001$.

potential protein (TRP) and its homologs are polypeptide subunits that assemble into tetramers to form cation channels activated by sensing diverse stimuli from the extracellular environment and from inside the cell[12]. Mammalian TRPs comprise six subfamilies[12]. TRPM2, a member of the TRPM subfamily, is a Ca^{2+}-permeable channel activated by intracellular messengers such as ADP-ribose (ADPR), nicotinamide adenine dinucleotide (NAD^+) and cyclic ADPR (cADPR)[13–15]. TRPM2 is abundantly expressed in inflammatory cells including monocytes, neutrophils and T lymphocytes[13–15]. We have reported that TRPM2 acts also as a sensor for ROS and oxidative stress[14]. However, the exact mediator molecules for H_2O_2-induced TRPM2 channel activation remain to be identified. The ROS sensitivity of TRPM2 can be mediated by NAD^+ (ref. 14) or ADPR[15] released from mitochondria[16] or through direct protein oxidation[15]. H_2O_2 and cADPR have been proposed to potentiate the effects of ADPR at lower concentrations and to gate the TRPM2 channel directly at higher concentrations[15]. It has been suggested that H_2O_2-activated Ca^{2+} influx through TRPM2 mediates pathophysiological cell death[14,17]. However, with regard to normal physiological cellular responses, the importance of H_2O_2-activated Ca^{2+} influx remains to be elucidated. It is crucial that the key roles of the TRPM2 channels be studied in the context of signaling mechanisms that control specific physiological responses.

Here we describe the functional role of TRPM2 in chemokine production. In U937 monocytes, Ca^{2+} influx via H_2O_2-activated TRPM2 mediates amplification of Erk activation and NF-κB nuclear translocation, which leads to CXCL8 production. In dextran sulfate sodium (DSS)-induced experimental colitis, which we employed as an inflammation model[18] associated with ROS[19,20], *Trpm2*-knockout mice showed attenuation of inflammatory indicators such as production of CXCL2, neutrophil infiltration and ulceration. Our study therefore suggests that ROS-evoked Ca^{2+} influx via TRPM2 represents a key inflammatory mediator in monocytes.

RESULTS

Ca^{2+} influx via TRPM2 controls H_2O_2-induced CXCL8 expression

In U937 cells, treatment with H_2O_2 induced mRNA expression and protein secretion of CXCL8 in a time- and dose-dependent manner (**Supplementary Fig. 1a**,**b** online). Consistent with previous reports[7,8,21,22], CXCL8 production was suppressed by the Erk pathway inhibitor PD98059 and the NF-κB inhibitor PDTC (**Fig. 1a**,**b** and **Supplementary Fig. 1c**). By contrast, H_2O_2-induced CXCL8 production was unaffected by the immunosuppressive agent FK506, which inhibits expression of chemokines such as CCL23 via nuclear factor of activated T cells (NFAT) in monocytes (**Supplementary Fig. 1d**,**e**).

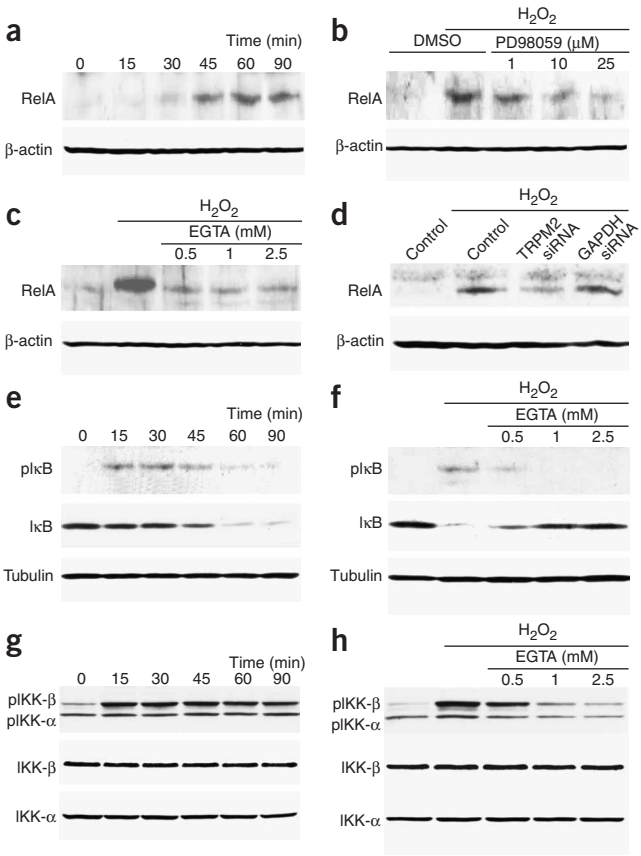

Figure 2 TRPM2-mediated Ca^{2+} influx controls H_2O_2-induced nuclear translocation of NF-κB via Erk in U937 cells. (**a**) Nuclear translocation of NF-κB RelA induced by incubation with 250 μM H_2O_2 as assessed at the indicated time points by western blotting. (**b**,**c**) Effects of PD98059 (**b**) and removal of extracellular Ca^{2+} by EGTA (**c**) on nuclear translocation of NF-κB after of 60 min H_2O_2 (250 μM) incubation. (**d**) Suppression of nuclear translocation of NF-κB by siRNA specific for TRPM2 after 60 min H_2O_2 (250 μM) incubation. (**e**) Time courses of phosphorylation and degradation of IκB induced by incubation with 250 μM H_2O_2. pIκB, phosphorylated IκB. (**f**) Effects of removal of extracellular Ca^{2+} by EGTA on phosphorylation and degradation of IκB induced by 250 μM H_2O_2 (60 min). (**g**) Time courses of phosphorylation of IKK-β and IKK-α (pIKK-β and pIKK-α) induced by incubation with 250 μM H_2O_2. (**h**) Effects of removal of extracellular Ca^{2+} by EGTA on phosphorylation of IKK-β and IKK-α induced by 250 μM H_2O_2 (60 min).

These results show that the Erk and NF-κB pathways control H_2O_2-induced CXCL8 production in U937 cells.

H_2O_2-induced CXCL8 production in U937 cells was reduced by removal of extracellular Ca^{2+} (**Fig. 1c**), and robust H_2O_2-evoked $[Ca^{2+}]_i$ increases were observed only after readdition of Ca^{2+} to external solution (**Fig. 1d**), suggesting that Ca^{2+} influx is key in H_2O_2-induced CXCL8 production. On the basis of our previous observation that TRPM2 shows the highest sensitivity to H_2O_2 in mediating Ca^{2+} influx among TRP homologs[14,23] and is abundantly expressed in monocytes[13,14], we tested the effects of TRPM2-specific small interfering RNA (siRNA; **Fig. 1e**). As a result, H_2O_2-induced $[Ca^{2+}]_i$ increases and CXCL8 production were reduced in TRPM2-specific siRNA-treated U937 cells (**Fig. 1f**,**g**), clearly suggesting an involvement of native TRPM2 in the Ca^{2+} influx that controls the H_2O_2-induced CXCL8 production in human monocytes.

TRPM2 mediates nuclear translocation of NF-κB

We next investigated whether Ca^{2+} influx via TRPM2 and Erk contribute to activation of NF-κB. Nuclear translocation of the NF-κB subunit RelA was triggered within 30 min of H_2O_2 stimulation and reached a maximum after 60 min (**Fig. 2a**). This RelA translocation was attenuated by PD98059 (**Fig. 2b**), by removal of extracellular Ca^{2+} (**Fig. 2c**), which also suppressed the H_2O_2-induced DNA-binding activity of RelA (**Supplementary Fig. 2a** online), and by TRPM2-specific siRNA (**Fig. 2d**). The phosphorylation and subsequent degradation of inhibitor of κB (IκB) and Erk-mediated phosphorylation of IκB kinase-β (IKK-β), responsible for RelA nuclear translocation, were also suppressed by removal of extracellular Ca^{2+} (**Fig. 2e–h**). By contrast, transcription levels of signaling components of the canonical NF-κB pathway (**Supplementary Fig. 2b**) and protein expression levels of IKK-β (**Fig. 2g**,**h**) were unaffected by H_2O_2 administration or by coapplication of PD98059. Furthermore, phosphorylation of IκB kinase-α (IKK-α; **Fig. 2g**,**h**) and processing of protein p100 into p52 and its nuclear translocation (**Supplementary Fig. 2c**,**d**), which is essential for the noncanonical NF-κB pathway[24], were insensitive to H_2O_2 and Ca^{2+} removal. Thus, H_2O_2-induced activation of the canonical NF-κB pathway is positively regulated by Erk and TRPM2-mediated Ca^{2+} influx in monocytes.

TRPM2 amplifies Erk signal via Pyk2 and Ras activation

Erk activation was induced by H_2O_2 within 2–5 min for Erk1 and 1 min for Erk2, reaching maximum levels after 10–20 min (**Fig. 3a**). After removal of extracellular Ca^{2+}, however, the activation of Erk1 was markedly reduced, although the Erk2 response to H_2O_2 was relatively intact (**Fig. 3a**). These results suggest that Ca^{2+} influx has a major role in Erk activation, reflected by the sustained phosphorylation of mainly Erk1 after 10–20 min of H_2O_2 stimulation (**Fig. 3a**). Much of this Ca^{2+} influx is probably mediated by TRPM2 channels, as H_2O_2-induced Erk1 activation was reduced by TRPM2-specific siRNA (**Fig. 3b**).

Ras, which represents an upstream signaling molecule of Erk, was gradually activated by H_2O_2, and its activation reached a plateau within 5 min, whereas this activation was abolished by removal of extracellular Ca^{2+} in U937 cells (**Fig. 3c**). A further upstream signaling molecule, the Ca^{2+}-sensitive, proline-rich tyrosine kinase Pyk2, is known to activate the Ras-Erk pathway[25]. Notably, a kinase-negative Pyk2 mutant (Pyk2-DN) that acts as a dominant negative[25] suppressed H_2O_2-evoked Ras and Erk activation (**Fig. 3d**). Erk activation was also suppressed by Pyk2-specific siRNAs (**Fig. 3e**), which suppressed nuclear translocation of NF-κB as well (**Fig. 3f**). Furthermore, the Pyk2 activation observed within 5 min of H_2O_2 stimulation was abolished by removal of extracellular Ca^{2+} (**Fig. 3g**) and was attenuated by TRPM2-specific siRNA (**Fig. 3h** and **Supplementary Fig. 2e**). However, siRNAs for two other candidate signaling molecules responsible for coupling of Ca^{2+} influx to Ras activation, RasGRP2 and RasGRP4, expressed in U937 cells[26] failed to inhibit H_2O_2-induced Erk activation (**Supplementary Fig. 2f**). We also examined two mitogen-activated protein kinases (MAPKs), JNK and p38-MAPK, activated by H_2O_2 with different time courses (**Supplementary Fig. 2g–j**). After removal of extracellular Ca^{2+}, JNK showed a slight delay but an intact maximal level of H_2O_2-induced activation, whereas p38-MAPK was essentially unaffected (**Supplementary Fig. 2g**,**h**). The p38-MAPK inhibitor SB203580 nearly abolished but the JNK inhibitor SP600125 failed to suppress H_2O_2-induced CXCL8 expression (**Supplementary Fig. 2i**,**j**). These data suggest that p38-MAPK contributes to H_2O_2-evoked CXCL8 expression independently of Ca^{2+}

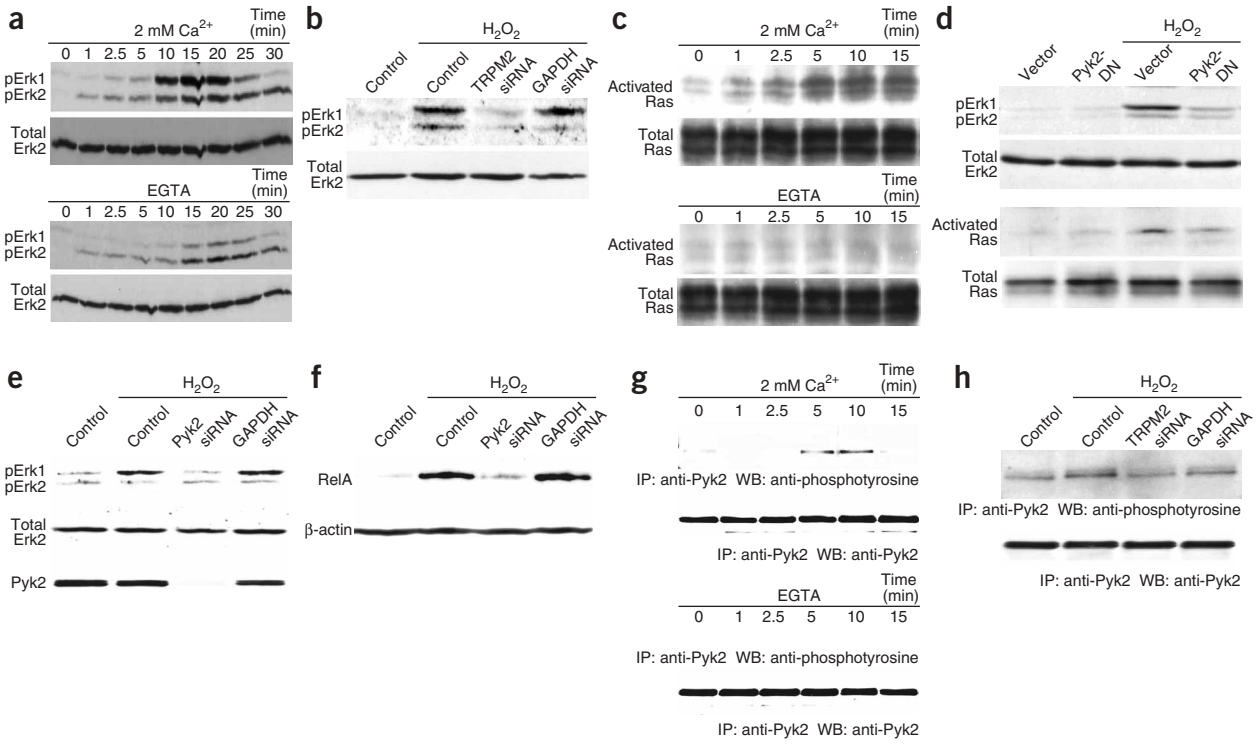

Figure 3 TRPM2-mediated Ca^{2+} influx activates Pyk2 and Ras to amplify Erk signal in U937 cells. (**a**) Erk activation induced by 250 μM H_2O_2 at the indicated time points of treatment in the presence (top) or absence (bottom) of extracellular Ca^{2+}. Activated Erk (pErk1 and pErk2: phosphorylated Erk1/2) is detected by phospho-Erk1/2–specific antibody. (**b**) Suppression of Erk activation by siRNA specific for TRPM2 after 10 min of H_2O_2 (250 μM) treatment. (**c**) Ras activation induced by 250 μM H_2O_2 at the indicated time points of treatment in the presence (top) or absence (bottom) of extracellular Ca^{2+}. (**d**) Inhibitory effects of Pyk2-DN on Erk (top) and Ras (bottom) activation after 10 min of H_2O_2 (250 μM) treatment. (**e**) Suppressive effects of Pyk2-specific siRNAs on Erk activation after 10 min of H_2O_2 (250 μM) treatment. (**f**) Suppressive effects of Pyk2-specific siRNAs on nuclear translocation of NF-κB RelA after 60 min of H_2O_2 (250 μM) incubation. (**g**) Pyk2 activation induced by 250 μM H_2O_2 at the indicated time points of treatment in the presence (top) or absence (lower panel) of extracellular Ca^{2+}. IP, immunoprecipitation; WB, western blotting; anti-Pyk2, antibody to Pyk2; anti-phosphotyrosine, antibody to phosphorylated tyrosine. (**h**) Suppressive effects of TRPM2-specific siRNA on Pyk2 activation after 10 min of H_2O_2 (250 μM) treatment.

influx. Thus, Ca^{2+} influx via H_2O_2-activated TRPM2 triggers Pyk2 and Ras activation, which then amplifies Erk activation, leading to nuclear translocation of NF-κB and CXCL8 production in U937 monocytes.

Trpm2 knockout disrupts chemokine production in monocytes

To study the physiological importance of TRPM2 channels and their *in vivo* effects on the signal transduction pathway revealed above, we generated transgenic mice in which TRPM2 expression was knocked out (**Supplementary Fig. 3a–c** online). *Trpm2*-knockout mice were viable, fertile and largely indistinguishable from wild-type (WT) littermates in general appearance, body weight, locomotion and overt behavior. Of note, a TRPM2 immunoreactivity that localized near the plasma membrane in monocytes from WT mice was absent in monocytes isolated from *Trpm2*-knockout mice (**Fig. 4a**). In monocytes obtained from WT mice, intracellular perfusion with increasing concentrations of ADPR evoked cationic currents (**Fig. 4b**). Monocytes isolated from *Trpm2*-knockout mice failed to respond entirely, and no substantial changes in current were ever observed (**Fig. 4c,d**). Similarly, WT monocytes typically responded to H_2O_2 by robust increases in cationic current (**Fig. 4e,f**) and $[Ca^{2+}]_i$ (**Fig. 4g**), whereas these phenotypes were nearly abolished in *Trpm2*-knockout monocytes (**Fig. 4e–g**). The $[Ca^{2+}]_i$ response defect was restored by cDNA transfection of TRPM2 but not by transfection of a cDNA encoding a TRPM2 mutant lacking the MutT motif essential for the action of the activators (**Supplementary Fig. 3d**)[13,14]. With regard to other types of cationic currents, Mg^{2+}- and ATP-regulated TRPM7-like current as well as Ca^{2+}-release activated Ca^{2+} current and Ca^{2+} influx evoked by store depletion were intact in *Trpm2*-knockout monocytes (**Supplementary Fig. 3e–g**).

As reported for the mouse macrophage cell line B10R (ref. 27), exposure of monocytes to 25 μM H_2O_2 induced expression of CXCL2 in WT cells, whereas this was impaired in mutant monocytes (**Fig. 5a**). CXCL2 expression induced by the endotoxin lipopolysaccharide and tumor necrosis factor-α, known as physiological stimulators of the ROS pathway[28], was also suppressed in *Trpm2*-knockout monocytes (**Supplementary Fig. 4a** online). In contrast, knockout of *Trpm2* did not affect expression of other cytokines sensitive (IL-1β, CCL2, CCL3, CCL4 and CXCL12) and insensitive (CCL1 and CCL21) to H_2O_2 induction in mouse monocytes (**Supplementary Fig. 4b**). With regard to H_2O_2-induced activation, Pyk2, Erk and IKK (**Fig. 5b**), but not the noncanonical NF-κB pathway, p38-MAPK and JNK (**Supplementary Fig. 4c–e**), were impaired in *Trpm2*-knockout monocytes. These data, together with suppression of H_2O_2-induced CXCL2 expression by the Erk and NF-κB inhibitors (**Fig. 5c**), strongly suggest that the H_2O_2-induced signaling cascade proposed for CXCL8 in U937 cells is applicable to CXCL2 in mouse monocytes[29]. The crucial contribution of NF-κB to RNA expression of CXCL2 has been also reported previously in comparison with other chemokines[27].

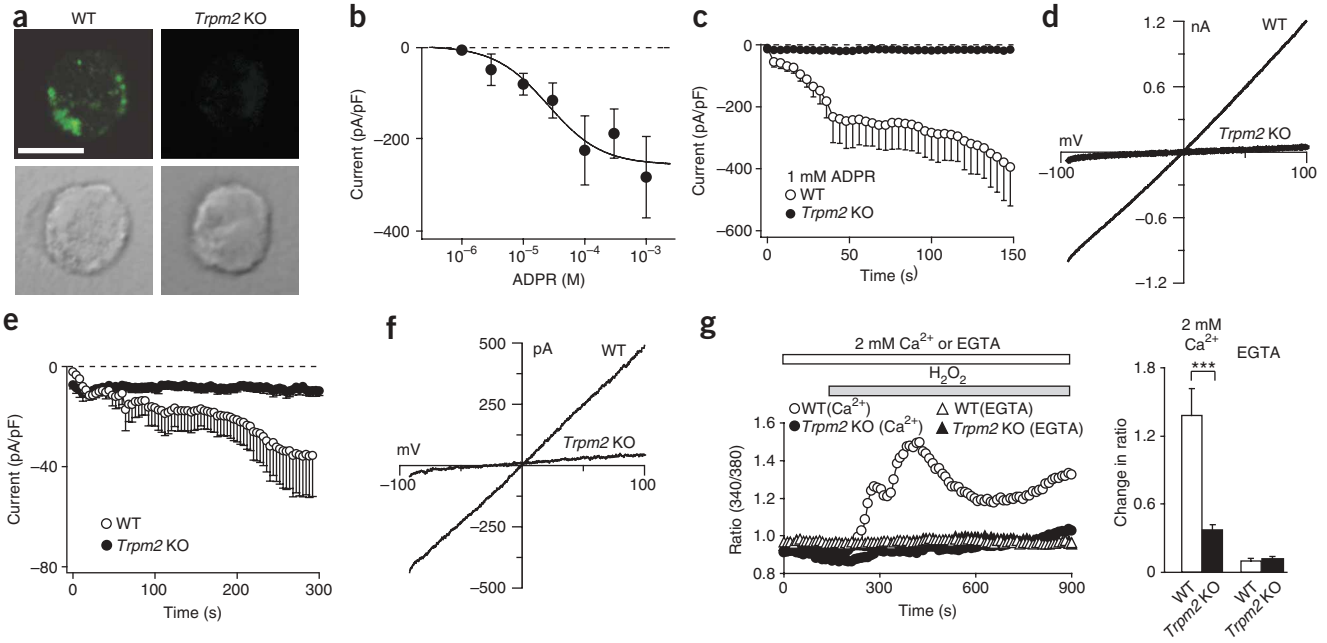

Figure 4 TRPM2 currents activated by ADPR and H_2O_2 are disrupted in *Trpm2*-knockout monocytes. (**a**) Confocal images of immunostaining with TRPM2-specific antibody (top) and differential interference contrast images (bottom) of *Trpm2*-knockout (KO) monocytes. Scale bar, 5 μm. (**b**) Dose-response curve of currents induced by internal perfusion with ADPR in WT monocytes. Current amplitudes are measured at –80 mV and 100 s, normalized for cell size, averaged and plotted against the respective ADPR concentrations ($n = 5$–7). A fit to the data points calculates the K_d at 25 μM with a Hill coefficient of 1. (**c**) Time course of current development induced at –80 mV by intracellular perfusion of WT ($n = 6$) or *Trpm2*-KO monocytes ($n = 11$) with 1 mM ADPR. (**d**) Representative current-voltage relationship obtained by a 50-ms voltage ramp pulse (–100 mV to +100 mV) from WT or *Trpm2*-KO monocytes after 100 s of ADPR perfusion. (**e**) Averaged current development induced at –80 mV by intrapipette H_2O_2 (100 μM) in WT ($n = 8$) or *Trpm2*-KO monocytes ($n = 11$). (**f**) Representative current-voltage relationship in WT or *Trpm2*-KO monocytes after 300 s of H_2O_2 perfusion. (**g**) Averaged time courses of $[Ca^{2+}]_i$ changes (left) and maximum $[Ca^{2+}]_i$ elevation (right) induced by 25 μM H_2O_2 in WT ($n = 24$) or *Trpm2*-KO ($n = 59$) monocytes in Ca^{2+}-containing or Ca^{2+}-free 0.5 mM EGTA-containing solution. Data points are means ± s.e.m. $^{***}P < 0.001$.

In vitro neutrophil migration toward the conditioned medium collected from WT monocyte cultures was significantly ($P < 0.01$) increased by H_2O_2 pretreatment, whereas this effect of H_2O_2 was nearly abolished when medium from *Trpm2*-knockout monocytes was used (**Fig. 5d**) or when neutralizing monoclonal antibody to CXCL2 was added to the WT medium (**Fig. 5e**). Thus, the differences of H_2O_2-induced CXCL2 expression observed in WT and *Trpm2*-knockout monocytes can influence the chemoattractant properties of

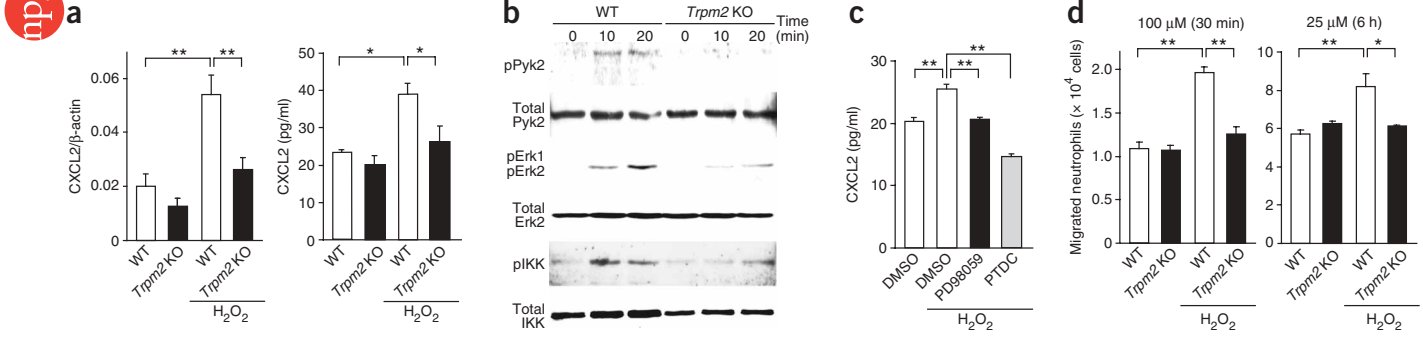

Figure 5 H_2O_2-induced CXCL2 production and the underlying signal transduction are impaired in *Trpm2* KO monocytes. (**a**) Expression levels of CXCL2 mRNA (left, real-time PCR) and CXCL2 protein secretion (right, ELISA) in monocytes isolated from WT or *Trpm2*-KO mice after treatment with 25 μM H_2O_2 for 3 h and 6 h, respectively. (**b**) Pyk2, Erk and NF-κB pathway activation induced by 25 μM H_2O_2 at the indicated time points of treatment in monocytes isolated from peripheral blood of WT and *Trpm2*-KO mice. (**c**) Inhibitory effects of Erk pathway inhibitor PD98059 and NF-κB inhibitor PDTC on H_2O_2 (25 μM)-induced expression of CXCL2 protein. (**d**) *In vitro* migration of neutrophils from WT mice by chemokines released from H_2O_2-treated monocytes isolated from WT or *Trpm2*-KO mice. Monocytes were cultured in the presence or absence of 100 μM H_2O_2 for 30 min (left) or 25 μM H_2O_2 for 6 h (right). After centrifugation of the cell suspension, the cells were resuspended in medium without H_2O_2 and incubated for 12 h (left) or 6 h (right). After removal of the cells by centrifugation, the supernatant derived from the culture medium was used in a neutrophil chemotaxis assay. (**e**) Inhibitory effects of neutralizing monoclonal antibody to CXCL2 on neutrophil chemotaxis induced by chemokines released from 25 μM H_2O_2-treated WT monocytes. Antibody to CXCL2 or isotype control (IgG2B) was added to the culture medium. Data points are means ± s.e.m. $^{*}P < 0.05$ and $^{**}P < 0.01$.

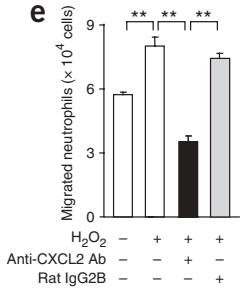

monocytes and affect neutrophil migration. Notably, however, we did not observe statistically significant differences in CXCL2-induced Ca^{2+} responses and *in vitro* migration between WT and *Trpm2*-knockout neutrophils (**Supplementary Fig. 5a**,**b** online), suggesting that CXCL2-induced responses in neutrophils are not dependent on TRPM2 activation. This is in contrast to Ca^{2+} responses and migration induced by a potent granulocyte chemoattractant, formyl-methionyl-leucyl-phenylalanine (fMLP) (**Supplementary Fig. 5c**,**d**).

Ulcerative colitis is suppressed in *Trpm2*-knockout mice

To establish the physiological significance *in vivo* of TRPM2-mediated CXCL2 production in ROS-stimulated monocytes, we examined the DSS model, in which mice show acute colitis characterized by epithelial injury and an acute inflammatory infiltrate[18] and many symptoms similar to those seen in human ulcerative colitis, that is, diarrhea, bloody feces, body weight loss, mucosal ulceration and shortening of colon[18,19]. In the DSS model, enhanced ROS release[19,20] and CXCL2 secretion have been reported to exacerbate ulcerative colitis[30]. As expected, expression of CXCL2 was greatly increased both in monocytes and in colon of DSS-treated WT mice, whereas CXCL2 expression was strongly suppressed in DSS-treated *Trpm2*-knockout mice (**Fig. 6a**,**b**). The proinflammatory cytokines interferon-γ (IFN-γ) and IL-12 (a potent IFN-γ inducer released from macrophages) were also significantly ($P < 0.01$) suppressed (**Supplementary Fig. 6** online). In contrast, knockout of *Trpm2* did not diminish expression in the colon of IL-6, IL-10, CCL1, CCL2, CCL3 and CCL5 (**Supplementary Fig. 6a–c**); the phenotypes of *in vitro* migration induced by CCL1, CCL2, CCL3, and CCL5 were intact in neutrophils and monocytes (**Supplementary Fig. 5e**,**f**). Notably, the number of recruited GR1-positive neutrophils was markedly reduced in DSS-treated *Trpm2*-knockout mice, whereas the number of macrophages ($F4/80^+$ or $CD11b^+Ly6C^{high}Ly6G^{low}$ cells) after infiltration into tissues was indistinguishable between WT and *Trpm2*-knockout mice (**Fig. 6c**,**d** and **Supplementary Fig. 6d**,**e**). Myeloperoxidase activity,

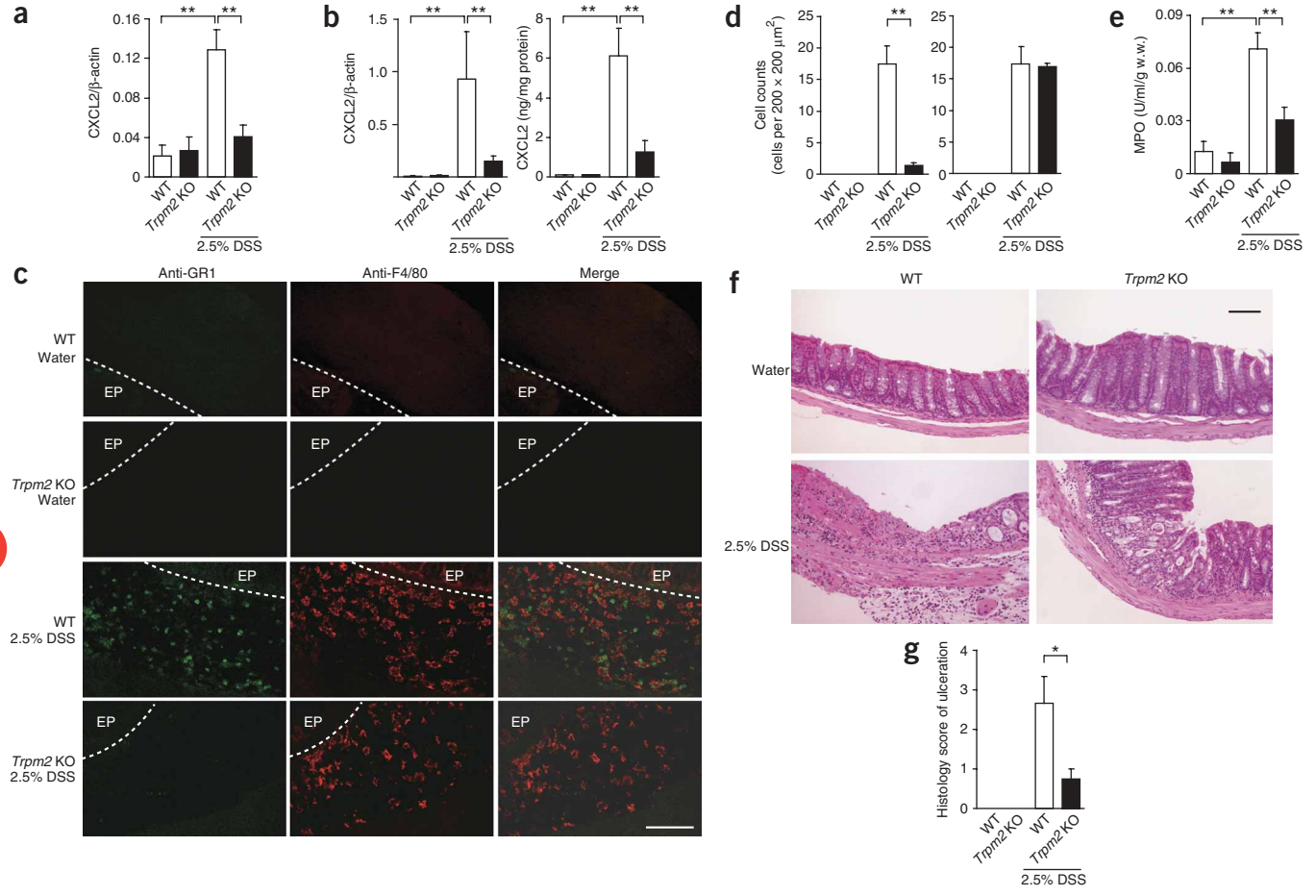

Figure 6 *Trpm2* deficiency suppresses exacerbation of inflammation in colitis mouse model. (**a**,**b**) Suppression of DSS-induced CXCL2 expression in *Trpm2*-KO mice. (**a**) CXCL2 expression levels of mRNA in monocytes isolated from peripheral blood. (**b**) Expression levels of CXCL2 mRNA (left) and protein (right) in the colon. (**c**) Dual immunofluorescent staining of colon tissue is performed with FITC-conjugated mouse GR1-specific antibody (anti-GR1, green) and R-PE–conjugated mouse F4/80-specific antibody (anti-F4/80, red). Submucosal and muscular layer and epithelium (EP) are shown. Water-treated WT, water-treated *Trpm2*-KO, DSS-treated WT and DSS-treated *Trpm2*-KO colons were used. Scale bar, 100 μm. (**d**) Cell counts of GR1-positive neutrophils (left) and F4/80-positive macrophages (right) in the colons of control and DSS-treated WT or *Trpm2*-KO mice (cells per 200 × 200 μm^2). (**e**) Activity of myeloperoxidase (MPO) in the colons of WT and *Trpm2*-KO mice. Data are normalized to colon wet weight (g w.w.). (**f**) H&E staining of colons isolated from water- or DSS-treated mice are shown, representing morphological findings for colons with histological score of ulceration. The histological scores of ulceration in the water-treated WT, water-treated *Trpm2*-KO, DSS-treated WT and DSS-treated *Trpm2* KO colons shown are 0, 0, 3 and 0, respectively. Scale bar, 1 mm. (**g**) Histology scores with respect to ulceration on a scale of 0–3 of WT or *Trpm2*-KO mice. Data points are mean ± s.e.m. $*P < 0.05$ and $**P < 0.01$.

an indicator of neutrophil infiltration after induction of colitis, was also reduced in DSS-treated *Trpm2*-knockout colon (**Fig. 6e**). This defect was restored by transfer of WT macrophages and TRPM2- or CXCL2-specific cDNA–transfected *Trpm2*-knockout macrophages derived from the bone marrow (**Supplementary Fig. 7** online).

It is noteworthy that *Trpm2*-knockout neutrophils retained *in vivo* neutrophil functions, which include infiltration of neutrophils introduced by bone marrow cell transfer into the DSS-treated colon (the ratio of infiltrated WT over *Trpm2*-knockout neutrophils was 0.96 ± 0.11 ($n = 5$); **Supplementary Fig. 8a**,**b** online) and bone marrow output and infiltration of neutrophils into the abdominal cavity after intraperitoneal injection of CXCL2 (**Supplementary Fig. 8c**). *In vivo* neutrophil output and infiltration elicited by intraperitoneal injection of CCL1, CCL3 and CCL5 was also intact in mutant mice, whereas that induced by fMLP was impaired in accordance with the *in vitro* migration data (**Supplementary Figs. 5d** and **8d**–**g**). *Trpm2*-knockout neutrophils showed partially impaired, yet significant ($P < 0.05$), bone marrow output in the DSS model (**Supplementary Fig. 8h**), which is consistent with the idea that bone marrow output is controlled by the balance between the chemoattractants released from the colon and those within the bone marrow. With regard to other immunocytes, T cells, dendritic cells and NK cells, DSS-induced infiltration was intact in *Trpm2*-knockout colon (**Supplementary Fig. 6f**). When introduced by bone marrow transfer, these immunocytes also showed intact colon infiltration (**Supplementary Fig. 8b**). These *in vivo* data, in combination with the intact *in vitro* migration of *Trpm2*-knockout neutrophils toward CXCL2 (**Supplementary Fig. 5b**), suggest that diminished expression of CXCL2 in macrophages contributes to the paucity of neutrophil accumulation in the colons of DSS-treated *Trpm2*-knockout mice.

Clinical assessments of disease activity showed profound inflammation and tissue destruction in the colon, characterized by mucosal ulceration, serosa destruction and infiltration of inflammatory cells in WT mice, whereas in *Trpm2*-knockout mice, the severity of the DSS-induced colitis was substantially reduced, although epithelial injury was identified (**Fig. 6f**,**g**). Moreover, *Trpm2*-knockout mice did not show DSS-induced loss of body weight and shortening of colon (**Supplementary Fig. 6g**,**h**). Thus, *Trpm2*-knockout mice were largely protected from DSS-mediated colitis, suggesting that TRPM2 has major roles in the progressive severity of inflammation.

DISCUSSION

The results of the present study show a key role of the Ca^{2+}-permeable channel TRPM2 in H_2O_2-induced chemokine production in monocytes that is of major physiological consequence in inflammation. Our *in vitro* studies in the human monocytotic cell line U937 suggest that H_2O_2 activates TRPM2 and amplifies downstream Ras and Erk signaling via Pyk2, leading to nuclear translocation of NF-κB and production of CXCL8. Our *in vivo* studies in *Trpm2*-knockout mice show that TRPM2 controls CXCL2 production in monocytes, which induces neutrophil migration and exacerbates DSS-induced ulcerative colitis.

It has been shown that Ras augments H_2O_2-induced CXCL8 production in experiments knocking down hypoxia inducible factor-1 (HIF-1), the transcription factor that controls scavenging of ROS in hypoxic conditions[22]. Of note, hypoxia-induced CXCL8 production via NF-κB activation is observed in HIF-1–deficient colon cancer DLD-1, which harbors an oncogenic *KRAS* mutation, but not in HIF-1–deficient colon cancer Caco2 cells carrying WT *KRAS*. This suggests that sustained activation of KRAS is crucial for H_2O_2-mediated CXCL8 production in colon cancer, which is consistent with the amplified Ras signal we observed for CXCL8 production in monocytes. With regard to other MAP kinases, the contribution of p38-MAPK to H_2O_2-induced CXCL8 expression is crucial but is independent of the TRPM2-mediated cascade, whereas the contribution of JNK is minimal, if any. This is consistent with the previously reported involvement of p38-MAPK in post-transcriptional regulation of CXCL8 expression[31].

NF-κB seems to be fully responsible for the H_2O_2-induced CXCL8 production in U937 cells (**Fig. 1b**), but H_2O_2-induced NF-κB nuclear translocation and CXCL8 production are partially TRPM2 and Mek independent (PD98059-insensitive) (**Figs. 1a**,**c**,**g** and **2b**–**d** and **Supplementary Fig. 1b**). A possible mechanism regarding Erk activation that could account for this observation might be a decrease in phosphatase activity, as protein tyrosine phosphatases (PTPs) can be inhibited by H_2O_2 (ref. 32). Specifically, inhibition of hematopoietic PTP (HePTP) expressed in U937 cells[33] might be involved, as HePTP inhibition has been reported to trigger Erk activation without Mek activation[32]. In addition, PTP inhibition positively regulates H_2O_2-evoked TRPM2 activation[34]. Therefore, some Erk activation through HePTP inhibition may be responsible for the residual nuclear translocation of NF-κB and CXCL8 production independent of TRPM2 and Mek. Notably, compared to Erk, the upstream Pyk2 showed more transient activation. This may be a result of H_2O_2-resistant PTPs that dephosphorylate and inactivate Pyk2.

At inflamed sites[4], multiple cells including neutrophils, macrophages and epithelial cells express NADPH oxidase, which generates ROS[3,4,35]. Cumulative evidence supports that ROS may function as mediators for aggravation of symptoms and pathophysiological responses in ulcerative colitis[19,20]. In mice, deficiency of nuclear factor erythroid-2–related factor-2 (Nrf2), a redox-sensitive transcriptional factor that regulates antioxidant genes[36], or an impaired superoxide dismutase activity[18] has been reported to increase susceptibility to DSS-induced colitis, indicating a major role of antioxidants in protecting the intestine against ROS in colitis. Notably, 100 μM H_2O_2 induced cell death in only 20% of U937 cells[14] but induced submaximal activation of CXCL8 transcription (nearly 80% maximum; **Supplementary Fig. 1b**). Hence, we hypothesize that moderate ROS exposure is a key signal for chemokine production and initiation of healing, whereas excessive ROS production and persistent Ca^{2+} entry may tilt the balance toward severe tissue damage and cell death.

CXCL2, similar to CXCL8 in humans, is one of the major inducible chemokines that lead to neutrophil infiltration[2] and subsequent tissue injury in several animal models of inflammation and injury, including ulcerative colitis[30,37,38]. Our results obtained from *Trpm2*-knockout mice fit well into this context, as mutant monocytes show impaired H_2O_2-induced expression of CXCL2. In contrast to CXCL2, keratinocyte-derived chemokine CXCL1, which also causes neutrophil chemotaxis[2], CCL19 and CXCL13 were undetectable in these cells (data not shown), and other cytokines tested were not susceptible to H_2O_2-inducted expression in mouse monocytes or showed intact H_2O_2-inducible expression in *Trpm2*-deficient monocytes. Therefore, the impaired *in vitro* neutrophil migration induced by conditioned medium containing chemokines from H_2O_2-treated *Trpm2*-knockout monocytes is probably attributable to reduced H_2O_2-induced CXCL2 expression. In monocytes and colon from DSS-treated *Trpm2*-knockout mice, CXCL2 expression is suppressed, whereas expression of IL-6, IL-10, CCL1, CCL2, CCL3 and CCL5 showed intact DSS inducibility. Inflammation parameters such as neutrophil infiltration and ulceration in the colon were also reduced in DSS-treated *Trpm2*-knockout mice. However, we did not observe statistically significant differences in DSS-induced macrophage recruitment between WT and

Trpm2-knockout colons. Notably, *Trpm2* deficiency did not impair key aspects of CXCL2-evoked neutrophil chemotaxis, including Ca^{2+} response, *in vitro* migration, *in vivo* infiltration after bone marrow transfer or in response to intraperitoneal CXCL2 injection, and bone marrow output. Recruitment of T cells, NK cells and dendritic cells also seemed intact in *Trpm2*-knockout colon. These results suggest that, overall, TRPM2 in macrophages accounts for much of the exacerbation of DSS-induced ulcerative colitis by mediating H_2O_2-triggered CXCL2 production and neutrophil infiltration. Nevertheless, it remains to be examined whether the *Trpm2* defect exerts effects widely on hematopoietic or nonhematopoietic cells, including epithelial cells, or on responses mediated by factors other than H_2O_2. In this context, it is noteworthy that DSS-induced expression of proinflammatory cytokines IFN-γ and IL-12 was diminished in the *Trpm2*-deficient colon, as these phenotypic changes that relieve tissue damage and inflammation are indicative of functional defects of monocyte-derived cells. Furthermore, neutrophilic Ca^{2+} responses and *in vitro* migration induced by fMLP and monocytotic CXCL2 expression induced by proinflammatory endotoxin lipopolysaccharide and cytokine tumor necrosis factor-α showed sensitivity but also some resistance to impairment by *Trpm2* knockout. Thus, future studies need to address relationships between multiple TRPM2-dependent and TRPM2-independent pathways in the complex *in vivo* DSS model and in human inflammatory diseases.

The tissue damage in human ulcerative colitis is probably mediated by neutrophils that have infiltrated the colonic mucosa, with CXCL8 representing the most potent specific neutrophil chemoattractant[39]. The degree of elevation of CXCL8 abundance is correlated with both disease activity and sigmoidoscopic severity in the dialysate bags[39] and with increased levels of infiltration of neutrophils in ulcerative colitis mucosa[40]. Notably, chronic inflammatory bowel diseases are mediated by activated monocytes and macrophages[41,42], whereas induction of CXCL8 expression is induced in the lamina propria macrophages of ulcerative colitis mucosa[43]. Kupffer cells, the resident liver macrophages, produce and release various proinflammatory cytokines, including CXCL8, leading to exacerbation of inflammatory liver disease[44], and CXCL8 produced by alveolar macrophages is involved in the development of chronic obstructive pulmonary disease[45]. By contrast, *in vivo* epithelial expression of CXCL8 is absent or minimal, although an *in vitro* capacity of epithelial cells to release CXCL8 has been demonstrated[43]. These studies, in combination with our *Trpm2*-knockout mouse studies, suggest a key role of CXCL8 produced by TRPM2 in monocytes and macrophages in the exacerbation of human ulcerative colitis. Of note, genetic links between TRPM2 and defective inflammatory diseases such as amyotrophic lateral suclerosis and parkinsonism dementia have been suggested[46]. Therefore, it is conceivable that CXCL8 production via TRPM2 triggers various inflammatory responses. This raises the prospect that suppression of CXCL8 production by inhibition of TRPM2 might be an effective way to reduce pathological severity in ulcerative colitis and many other inflammatory diseases related to ROS production.

ADPR may be a major messenger molecule that links ROS to TRPM2 activation and Ca^{2+} entry in inflammation, because excessive oxidative stress leads to enzymatic ADPR production in inflammatory chemokine production[47–49] and ADPR mobilization from mitochondria[16]. In immunocytes, including neutrophils, CD38 produces cADPR and ADPR[50]. CD38-deficient neutrophils have disturbed Ca^{2+} signaling and chemotaxis in response to fMLP via fMLP receptors[50]. Notably, the fMLP-induced Ca^{2+} response and *in vitro* migration were suppressed in *Trpm2*-deficient neutrophils. This supports the idea that fMLP activates CD38 to induce cADPR and ADPR production and the Ca^{2+} influx via TRPM2 required for neutrophil chemotaxis[15], in contrast to the CXCL2-induced neutrophil chemotaxis that does not receive a significant contribution from TRPM2 channels and that is probably mediated by classical inositol triphosphate-induced Ca^{2+} release and possibly store-operated Ca^{2+} entry. It will be useful to study which type of signaling mechanism other chemokines employ in inducing chemotaxis.

METHODS

Isolation of mouse monocytes. We isolated monocytes from peripheral blood mononuclear cells by CD11b positivity using a magnetic sorting system. All animal experiments were performed in accordance with protocols approved by the Institutional Animal Care and Use Committees of the Graduate School of Engineering, Kyoto University. For details, see **Supplementary Methods** online.

Northern blot analysis. We carried out hybridization with cDNA probes for TRPM2, CXCL8 or 18S rRNA. For details, see **Supplementary Methods**.

Determination of human CXCL8 and mouse CXCL2 concentration. We determined concentrations of human CXCL8 from U937 cells and CXCL2 from mouse monocytes or colons by ELISA according to the manufacturers' instructions (Endogen and R&D Systems, respectively).

Small interfering RNA. We used the TRPM2 siRNA sequence targeting the coding region of TRPM2 mRNA (5′-AAAGCCTCAGTTCGTGGATTC-3′) and the Pyk2 siRNA sequences targeting the coding region of Pyk2 mRNA (5′-AATGCACTTGACAAGAAGTCC-3′), (5′-AAGATGTGGTCCTGAATCGTA-3′), (5′-AAGGTGTCTACACAAATCACA-3′), and (5′-AAGTCCCTGGACCCCATGGTT-3′). We used cells 48 h after siRNA transfection. We used an siRNA directed against glyceraldehyde-3-phosphate dehydrogenase (GAPDH) as a control. For details, see **Supplementary Methods**.

Measurement of changes in intracellular calcium concentration. We measured changes in $[Ca^{2+}]_i$ as previously described[23]. We measured the fura-2 fluorescence in HEPES-buffered saline containing (in mM): 107 NaCl, 6 KCl, 1.2 $MgSO_4$, 2 $CaCl_2$, 11.5 glucose and 20 HEPES (pH 7.4, adjusted with NaOH). We obtained the 340:380 nm ratio images on a pixel-by-pixel basis.

Nuclear translocation of nuclear factor-κB. We determined nuclear translocation of NF-κB by western blotting. We detected the total amount of β-actin as the loading control. For details, see **Supplementary Methods**.

Western blot analysis. We determined activation of Erk, Pyk2, IκB, IKK-β, IKK-α and degradation of IκB by western blotting. For details, see **Supplementary Methods**.

Ras-GTP assay. We prebound bacterially expressed GST-Ras binding domain (amino acids 1–149 of human cRaf-1 fused to GST) to glutathione-conjugated beads and incubated the beads with each cell lysate. We subjected bound proteins to western blotting. For details, see **Supplementary Methods**.

Pyk2 activation assay. We immunoprecipitated cell lysates for 2 h at 4 °C with protein A–agarose linked to Pyk2-specific antibody (Upstate). We analyzed immunoprecipitates by western blotting with phosphotyrosine-specific antibody (Upstate). Details of the procedure for immunoprecipitation are described in **Supplementary Methods**.

Confocal immunovisualization in isolated monocytes. We fixed monocytes with paraformaldehyde, immunostained them with TRPM2-specific antibody (1:100 mLTRPC2-C1; ref. 14) and visualized them with the Alexa Fluor 488–conjugated rabbit IgG-specific antibody (Invitrogen) to detect TRPM2. We acquired the fluorescence images with a confocal laser-scanning microscope (Olympus FV500) using the 488-nm line of an argon laser for excitation and a 505-nm long-pass filter for emission.

Electrophysiology. We performed patch-clamp experiments in the whole-cell configuration. We kept cells in standard Ringer's solution (in mM):

140 NaCl, 2.8 KCl, 1 $CaCl_2$, 2 $MgCl_2$, 10 glucose and 10 HEPES-NaOH (pH 7.2 adjusted with NaOH). Standard pipette-filling solutions contained (in mM): 140 Cs-glutamate, 8 NaCl, 1 $MgCl_2$ and 10 HEPES-CsOH (pH 7.2 adjusted with CsOH). We left Ca^{2+} unbuffered by leaving out any calcium chelator. We acquired all data with Pulse software controlling an EPC-9 amplifier (HEKA) and analyzed with FitMaster (HEKA) and Igor Pro (Wavemetrics). For details, see **Supplementary Methods**.

Real-time PCR. After reverse-transcription to cDNA from total RNA, we performed quantification by real-time PCR (LightCycler instrument, Roche) using the LightCycler FastStart DNA Master HybProbe Kit (Roche). We normalized the results for CXCL2 relative to β-actin expression. For details, see **Supplementary Methods**.

Isolation of bone marrow neutrophils. We isolated mouse bone marrow neutrophils from femurs and tibias by Percoll density gradient centrifugation. We lysed the remaining erythrocytes with buffer containing (in mM): 150 NH_4Cl, 1 $KHCO_3$ and 0.1 Na_2EDTA. For details, see **Supplementary Methods**.

***In vitro* migration assay.** We used 6.5-mm diameter well chambers with 3-μm pore size membranes (Costar) to determine neutrophil chemotaxis. We added the tested supernatants to the lower chamber. We allowed neutrophils (5×10^5 cells) isolated from bone marrow to migrate from the upper to the lower chamber for 1.5 h and then counted the number of migrating cells. We added CXCL2-specific antibody (R&D Systems) or isotype control antibody IgG2B (MBL) to the culture medium in the lower chamber.

Induction of colitis by dextran sulfate sodium. We gave mice sterile distilled water containing 2.5% DSS (molecular weight 36,000–50,000) *ad libitum* throughout the experiment.

Immunofluorescent staining of colon sections. We placed colon specimens in Tissue-Tek optimum cutting-temperature compound (Sakura), snap-froze them in dry ice and ethanol and stored them at –80 °C. After fixation and rehydration, we then incubated samples with R-phycoerythrin (R-PE)-conjugated mouse F4/80-specific antibody (Serotec) and FITC-conjugated mouse GR1-specific antibody (BD Pharmingen). We acquired the fluorescence images with a confocal laser-scanning microscope and counted the numbers of GR1-positive neutrophils and F4/80-positive macrophages in the images. For details, see **Supplementary Methods**.

Myeloperoxidase assay. After freeze-and-thaw and centrifugation of homogenized colon specimens, we mixed 100 μl of supernatant with a solution of 0.167 mg ml^{-1} *O*-dianisidine hydrochloride and 0.0005% H_2O_2. We measured myeloperoxidase activity spectrophotometrically as the change in absorbance at 460 nm. For details, see **Supplementary Methods**.

Histological evaluation of colonic lesions. We stained colon sections fixed with formalin and embedded in paraffin with H&E for the morphological evaluation. We graded the histopathological change on a scale from 0 to 3 according to the following criteria: 0, no remarkable change; 1, slight change; 2, moderate change; and 3, marked change. We calculated the histological score of ulceration by adding each score for proximal, middle and distal colon. For details, see **Supplementary Methods**.

Statistical analyses. All data are expressed as means ± s.e.m. We accumulated the data for each condition from at least three independent experiments. We evaluated statistical significance with the Student's *t*-test for comparisons between two mean values. We carried out multiple comparisons between more than three groups with an ANOVA followed by Tukey-Kramer test.

Note: Supplementary information is available on the Nature Medicine website.

ACKNOWLEDGMENTS

We thank T. Niidome, T. Nakagawa and H. Shirakawa for their support in mouse experiments and M. Hikida, T. Yamazaki and K. Takahara for helpful advice. This study was supported by research grants from the Ministry of Education, Culture, Sports, Science, and Technology of Japan, the Japan Society for the Promotion of Science, Japan Science and Technology Agency, and the US National Institutes of Health.

AUTHOR CONTRIBUTIONS

S.Y., acquisition, analysis and interpretation of data and drafting of the manuscript; S.S., S. Kiyonaka, N.T., T.W., Y.H., T.N., T.H., T.O., I.L., A.F. and M.N., acquisition, analysis and interpretation of data; Y.K., S. Kaneko, R.P. and H.T., analysis and interpretation of data; Y.M., analysis and interpretation of data and drafting and critical review of the manuscript.

Published online at http://www.nature.com/naturemedicine/
Reprints and permissions information is available online at http://npg.nature.com/reprintsandpermissions/

1. Luster, A.D. Chemokines—chemotactic cytokines that mediate inflammation. *N. Engl. J. Med.* **338**, 436–445 (1998).
2. Sonoda, Y. *et al.* Physiologic regulation of postovulatory neutrophil migration into vagina in mice by a C-X-C chemokine(s). *J. Immunol.* 6159–6165 (1998).
3. Fialkow, L., Wang, Y. & Downey, G.P. Reactive oxygen and nitrogen species as signaling molecules regulating neutrophil function. *Free Radic. Biol. Med.* **42**, 153–164 (2007).
4. Henricks, P.A.J. & Nijkamp, F.P. Reactive oxygen species as mediators in asthma. *Pulm. Pharmacol. Ther.* **14**, 409–421 (2001).
5. Dröge, W. Free radicals in the physiological control of cell function. *Physiol. Rev.* **82**, 47–95 (2002).
6. Cavaillon, J.M. & Adib-Conquy, M. Monocytes/macrophages and sepsis. *Crit. Care Med.* **33**, S506–S509 (2005).
7. Josse, C., Boelaert, J.R., Best-Belpomme, M. & Piette, J. Importance of post-transcriptional regulation of chemokine genes by oxidative stress. *Biochem. J.* **360**, 321–333 (2001).
8. Zeng, X., Dai, J., Remick, D.G. & Wang, X. Homocysteine mediated expression and secretion of monocyte chemoattractant protein-1 and interleukin-8 in human monocytes. *Circ. Res.* **93**, 311–320 (2003).
9. Feske, S., Giltnane, J., Dolmetsch, R., Staudt, L.M. & Rao, A. Gene regulation mediated by calcium signals in T lymphocytes. *Nat. Immunol.* **2**, 316–324 (2001).
10. Wilson, L., Butcher, C.J. & Kellie, S. Calcium ionophore A23187 induces interleukin-8 gene expression and protein secretion in human monocytic cells. *FEBS Lett.* **325**, 295–298 (1993).
11. Méndez-Samperio, P., Palma-Barrios, J., Vázquez-Hernández, A. & García-Martinez, E. Secretion of interleukin-8 by human-derived cell lines infected with *Mycobacterium bovis*. *Mediators Inflamm.* **13**, 45–49 (2004).
12. Clapham, D.E. TRP channels as cellular sensors. *Nature* **426**, 517–524 (2003).
13. Perraud, A.L. *et al.* ADP-ribose gating of the calcium-permeable LTRPC2 channel revealed by Nudix motif homology. *Nature* **411**, 595–599 (2001).
14. Hara, Y. *et al.* LTRPC2 Ca^{2+}-permeable channel activated by changes in redox status confers susceptibility to cell death. *Mol. Cell* **9**, 163–173 (2002).
15. Massullo, P., Sumoza-Toledo, A., Bhagat, H. & Partida-Sánchez, S. TRPM channels, calcium and redox sensors during innate immune responses. *Semin. Cell Dev. Biol.* **17**, 654–666 (2006).
16. Perraud, A.L. *et al.* Accumulation of free ADP-ribose from mitochondria mediates oxidative stress–induced gating of TRPM2 cation channels. *J. Biol. Chem.* **280**, 6138–6148 (2005).
17. Kaneko, S. *et al.* A critical role of TRPM2 in neuronal cell death by hydrogen peroxide. *J. Pharmacol. Sci.* **101**, 66–76 (2006).
18. Korenaga, D. *et al.* Impaired antioxidant defense system of colonic tissue and cancer development in dextran sulfate sodium–induced colitis in mice. *J. Surg. Res.* **102**, 144–149 (2002).
19. Blackburn, A.C., Doe, W.F. & Buffinton, G.D. Salicylate hydroxylation as an indicator of hydroxyl radical generation in dextran sulfate–induced colitis. *Free Radic. Biol. Med.* **25**, 305–313 (1998).
20. Araki, Y., Sugihara, H. & Hattori, T. The free radical scavengers edaravone and tempol suppress experimental dextran sulfate sodium–induced colitis in mice. *Int. J. Mol. Med.* **17**, 331–334 (2006).
21. Chiu, L.L., Perng, D.W., Yu, C.H., Su, S.N. & Chow, L.P. Mold allergen, pen C 13, induces IL-8 expression in human airway epithelial cells by activating protease-activated receptor 1 and 2. *J. Immunol.* **178**, 5237–5244 (2007).
22. Mizukami, Y. *et al.* Induction of interleukin-8 preserves the angiogenic response in HIF-1α–deficient colon cancer cells. *Nat. Med.* **11**, 992–997 (2005).
23. Yoshida, T. *et al.* Nitric oxide activates TRP channels by cysteine S-nitrosylation. *Nat. Chem. Biol.* **2**, 596–607 (2006).
24. Dejardin, E. *et al.* The lymphotoxin-β receptor induces different patterns of gene expression via two NF-κB pathways. *Immunity* **17**, 525–535 (2002).
25. Lev, S. *et al.* Protein tyrosine kinase PYK2 involved in Ca^{2+}-induced regulation of ion channel and MAP kinase functions. *Nature* **376**, 737–745 (1995).
26. Roose, J.P., Mollenauer, M., Gupta, V.A., Stone, J. & Weiss, A. A diacylglycerol-protein kinase C-RasGRP1 pathway directs Ras activation upon antigen receptor stimulation of T cells. *Mol. Cell. Biol.* **25**, 4426–4441 (2005).
27. Jaramillo, M. & Olivier, M. Hydrogen peroxide induces murine macrophage chemokine gene transcription via extracellular signal-regulated kinase– and cyclic adenosine 5′-monophosphate (cAMP)–dependent pathways: involvement of NF-κB, activator protein 1, and cAMP response element binding protein. *J. Immunol.* **169**, 7026–7038 (2002).
28. Gloire, G., Legrand-Poels, S. & Piette, J. NF-κB activation by reactive oxygen species: fifteen years later. *Biochem. Pharmacol.* **72**, 1493–1505 (2006).

29. Kim, D.-S., Han, J.H. & Kwon, H.J. NF-κB and c-Jun–dependent regulation of macrophage inflammatory protein-2 gene expression in response to lipopolysaccharide in RAW 264.7 cells. *Mol. Immunol.* **40**, 633–643 (2003).
30. Ohtsuka, Y. & Sanderson, I.R. Dextran sulfate sodium–induced inflammation is enhanced by intestinal epithelial cell chemokine expression in mice. *Pediatr. Res.* **53**, 143–147 (2003).
31. Saklatvala, J. The p38 MAP kinase pathway as a therapeutic target in inflammatory disease. *Curr. Opin. Pharmacol.* **4**, 372–377 (2004).
32. Lee, K. & Esselman, W.J. cAMP potentiates H_2O_2-induced ERK1/2 phosphorylation without the requirement for MEK1/2 phosphorylation. *Cell. Signal.* **13**, 645–652 (2001).
33. Seimiya, H. & Tsuruo, T. Differential expression of protein tyrosine phosphatase genes during phorbol ester–induced differentiation of human leukemia U937 cells. *Cell Growth Differ.* **4**, 1033–1039 (1993).
34. Zhang, W. *et al.* Regulation of TRP channel TRPM2 by the tyrosine phosphatase PTPL1. *Am. J. Physiol. Cell Physiol.* **292**, C1746–C1758 (2007).
35. Lambeth, J.D. NOX enzymes and the biology of reactive oxygen. *Nat. Rev. Immunol.* **4**, 181–189 (2004).
36. Khor, T.O. *et al.* Nrf2-deficient mice have an increased susceptibility to dextran sulfate sodium–induced colitis. *Cancer Res.* **66**, 11580–11584 (2006).
37. Han, X.B., Liu, X., Hsueh, W. & De Plaen, I.G. Macrophage inflammatory protein-2 mediates the bowel injury induced by platelet-activating factor. *Am. J. Physiol. Gastrointest. Liver Physiol.* **287**, G1220–G1226 (2004).
38. Buanne, P. *et al.* Crucial pathophysiological role of CXCR2 in experimental ulcerative colitis in mice. *J. Leukoc. Biol.* **82**, 1239–1246 (2007).
39. Keshavarzian, A. *et al.* Increased interleukin-8 (IL-8) in rectal dialysate from patients with ulcerative colitis: evidence for a biological role for IL-8 in inflammation of the colon. *Am. J. Gastroenterol.* **94**, 704–712 (1999).
40. Anezaki, K. *et al.* Correlations between interleukin-8, and myeloperoxidase or luminol-dependent chemiluminescence in inflamed mucosa of ulcerative colitis. *Intern. Med.* **37**, 253–258 (1998).
41. Grip, O., Janciauskiene, S. & Lindgren, S. Macrophages in inflammatory bowel disease. *Curr. Drug Targets Inflamm. Allergy* **2**, 155–160 (2003).
42. Smith, P.D., Ochsenbauer-Jambor, C. & Smythies, L.E. Intestinal macrophages: unique effector cells of the innate immune system. *Immunol. Rev.* **206**, 149–159 (2005).
43. Mahida, Y.R. The key role of macrophages in the immunopathogenesis of inflammatory bowel disease. *Inflamm. Bowel Dis.* **6**, 21–33 (2000).
44. Videla, L.A., Fernández, V., Tapia, G. & Varela, P. Oxidative stress–mediated hepatotoxicity of iron and copper: role of Kupffer cells. *Biometals* **16**, 103–111 (2003).
45. Barnes, P.J. COPD: is there light at the end of the tunnel? *Curr. Opin. Pharmacol.* **4**, 263–272 (2004).
46. Hermosura, M.C. & Garruto, R.M. *TRPM7* and *TRPM2*—candidate susceptibility genes for Western Pacific ALS and PD? *Biochim. Biophys. Acta* **1772**, 822–835 (2007).
47. Fonfria, E. *et al.* TRPM2 channel opening in response to oxidative stress is dependent on activation of poly(ADP-ribose) polymerase. *Br. J. Pharmacol.* **143**, 186–192 (2004).
48. Cuzzocrea, S. *et al.* Role of poly(ADP-ribose) glycohydrolase in the development of inflammatory bowel disease in mice. *Free Radic. Biol. Med.* **42**, 90–105 (2007).
49. Haskó, G. *et al.* Poly(ADP-ribose) polymerase is a regulator of chemokine production: relevance for the pathogenesis of shock and inflammation. *Mol. Med.* **8**, 283–289 (2002).
50. Partida-Sánchez, S. *et al.* Cyclic ADP-ribose production by CD38 regulates intracellular calcium release, extracellular calcium influx and chemotaxis in neutrophils and is required for bacterial clearance *in vivo*. *Nat. Med.* **7**, 1209–1216 (2001).

Supplementary Information

TRPM2-mediated Ca^{2+} influx induces chemokine production in monocytes that aggravates inflammatory neutrophil infiltration

Shinichiro Yamamoto, Shunichi Shimizu, Shigeki Kiyonaka, Nobuaki Takahashi, Teruaki Wajima, Yuji Hara, Takaharu Negoro, Toshihito Hiroi, Yuji Kiuchi, Takaharu Okada, Shuji Kaneko, Ingo Lange, Andrea Fleig, Reinhold Penner, Miyuki Nishi, Hiroshi Takeshima & Yasuo Mori

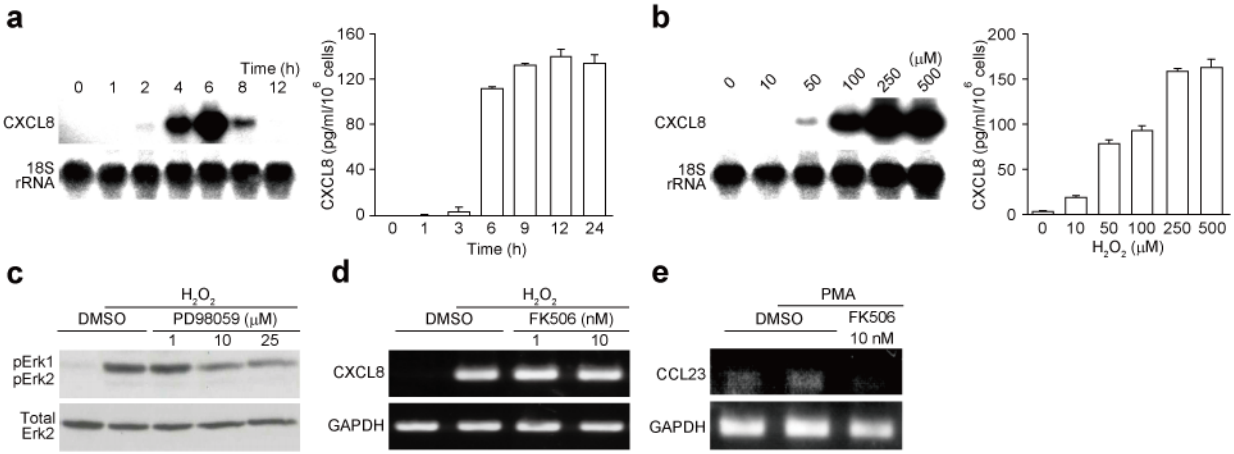

Supplementary Figure 1. H_2O_2-induced expression of CXCL8 in U937 cells. (**a**) Expression levels of CXCL8 mRNA (left panel, Northern blot analysis) and protein secretion (right panel, ELISA) induced by incubation with 250 μM H_2O_2 at indicated time points. (**b**) Expression of CXCL8 mRNA (left panel) and secretion (right panel) induced by incubation with H_2O_2 at different concentrations (0 to 500 μM) for 6 h and 12 h, respectively. (**c**) Inhibitory effects of Erk pathway inhibitor PD98059 on H_2O_2 (250 μM)-induced Erk activation. (**d,e**) NFAT-independent induction of CXCL8 expression by H_2O_2. Effects of NFAT pathway inhibitor FK506 on H_2O_2 (250 μM)-induced expression of CXCL8 mRNA (**d**) and PMA (20 ng ml^{-1})-induced expression of CCL23 mRNA (**e**) are examined. Data points are mean ± s.e.m..

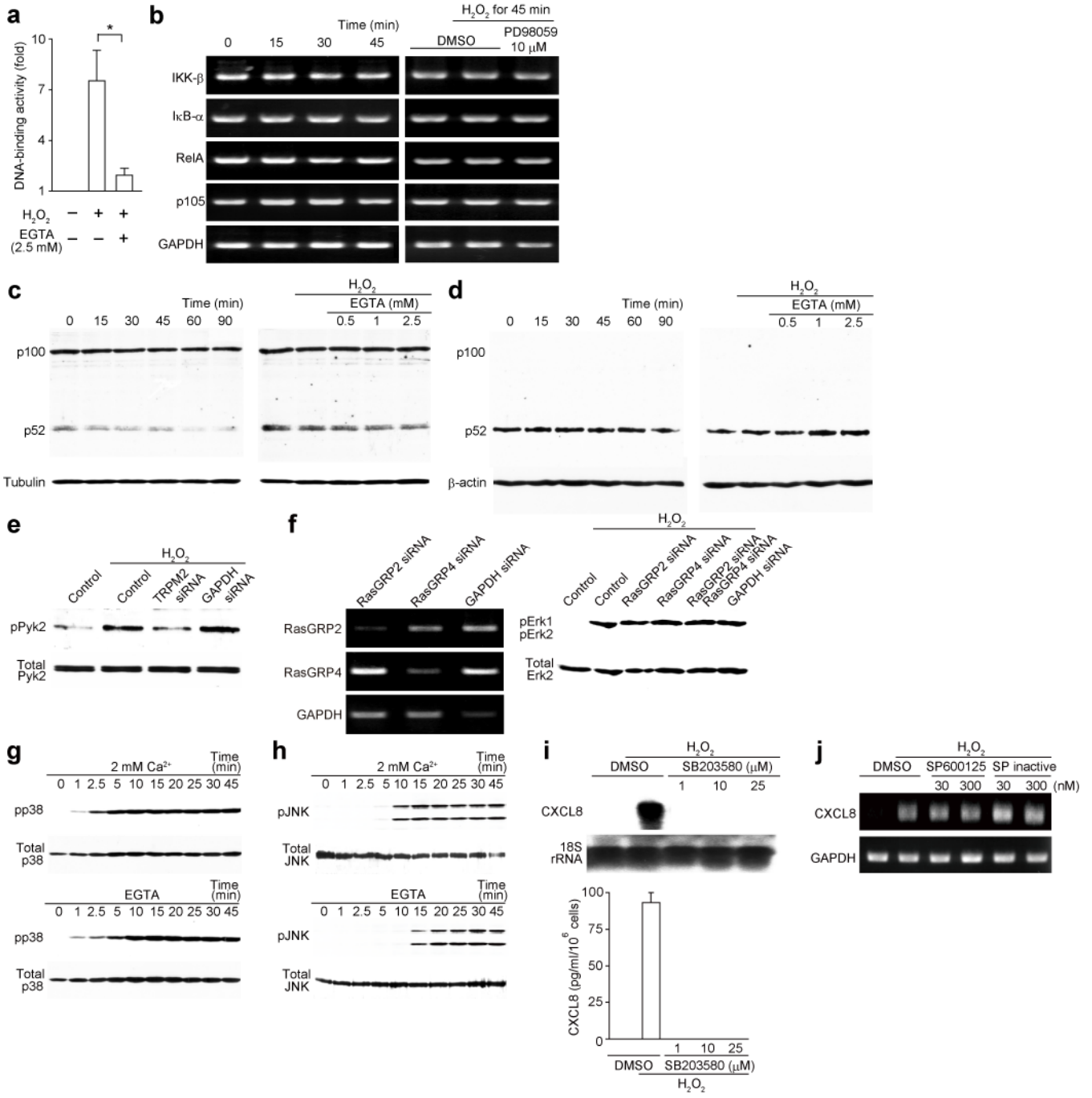

Supplementary Figure 2

Supplementary Figure 2. H_2O_2-induced signaling via TRPM2 in U937 cells. (**a–d**) H_2O_2 sensitivity of canonical and non-canonical NF-κB pathways in U937 cells. (**a**) Stimulation of DNA-binding activity of NF-κB (RelA) with 250 μM H_2O_2 for 90 min is measured by transcription factor ELISA. Data are presented as 'fold activation' relative to the level of NF-κB activation in unstimulated U937 cells. (**b**) Transcription of signaling proteins comprising the canonical NF-κB pathway upon application of H_2O_2 (250 μM). Time courses (left panel) and effects of co-application of the Erk pathway inhibitor PD98059 (right panel) are examined by RT-PCR. (**c**) Processing of the non-canonical NF-κB pathway protein p100 into p52 induced by incubation with 250 μM H_2O_2 is assessed at indicated time points by Western blot (left panel). Effects of omission of extracellular Ca^{2+} by EGTA on the p100 processing after 60 min H_2O_2 (250 μM) incubation (right panel). (**d**) Nuclear translocation of p52 induced by incubation with 250 μM H_2O_2 is assessed at indicated time points by Western blot (left panel). Nuclear translocation of p52 after omission of extracellular Ca^{2+} with EGTA by 60 min incubation with H_2O_2 (250 μM) (right panel). (**e**) Suppression of Pyk2 activation by siRNA for TRPM2 after 10 min H_2O_2 (250 μM) treatment in U937 cells. Phosphorylation of Pyk2 (pPyk2) is assessed by Western blot analysis using phospho-Pyk2-specific antibody. (**f**) Effects of siRNAs for RasGRP2 and RasGRP4 on H_2O_2-induced Erk activation in U937 cells. RasGRP2, RasGRP4, and GAPDH mRNA expression in cells transfected with siRNAs specific for RasGRP2, RasGRP4, and GAPDH, respectively are analyzed by RT-PCR (left panel). Erk activation after 10 min H_2O_2 (250 μM) treatment in cells transfected with siRNAs specific for RasGRP2, RasGRP4, or GAPDH (right panel). (**g–j**) H_2O_2-induced p38-MAPK and JNK activation in U937 cells. (**g**) p38-MAPK activation induced by 250 μM H_2O_2 at indicated time points of treatment in the presence (upper panel) or absence (lower panel) of extracellular Ca^{2+}. Activated p38-MAPK (pp38) is assessed by Western blot using phospho-p38-MAPK-specific antibody. (**h**) JNK activation induced by 250 μM H_2O_2 at indicated time points of treatment in the presence (upper panel) or absence (lower panel) of extracellular Ca^{2+}. Activated JNK (pJNK) is assessed by Western blot using phospho-JNK-specific antibody. (**i**) Inhibitory effects of p38-MAPK inhibitor SB203580 on H_2O_2 (250 μM)-induced expression of CXCL8 mRNA (upper panel) and secretion (lower panel). (**j**) Lack of significant effects of JNK inhibitor SP600125 and negative SP600125 control (SP inactive) on H_2O_2 (250 μM)-induced expression of CXCL8 mRNA (RT-PCR). Data points are mean ± s.e.m.. * $P < 0.05$.

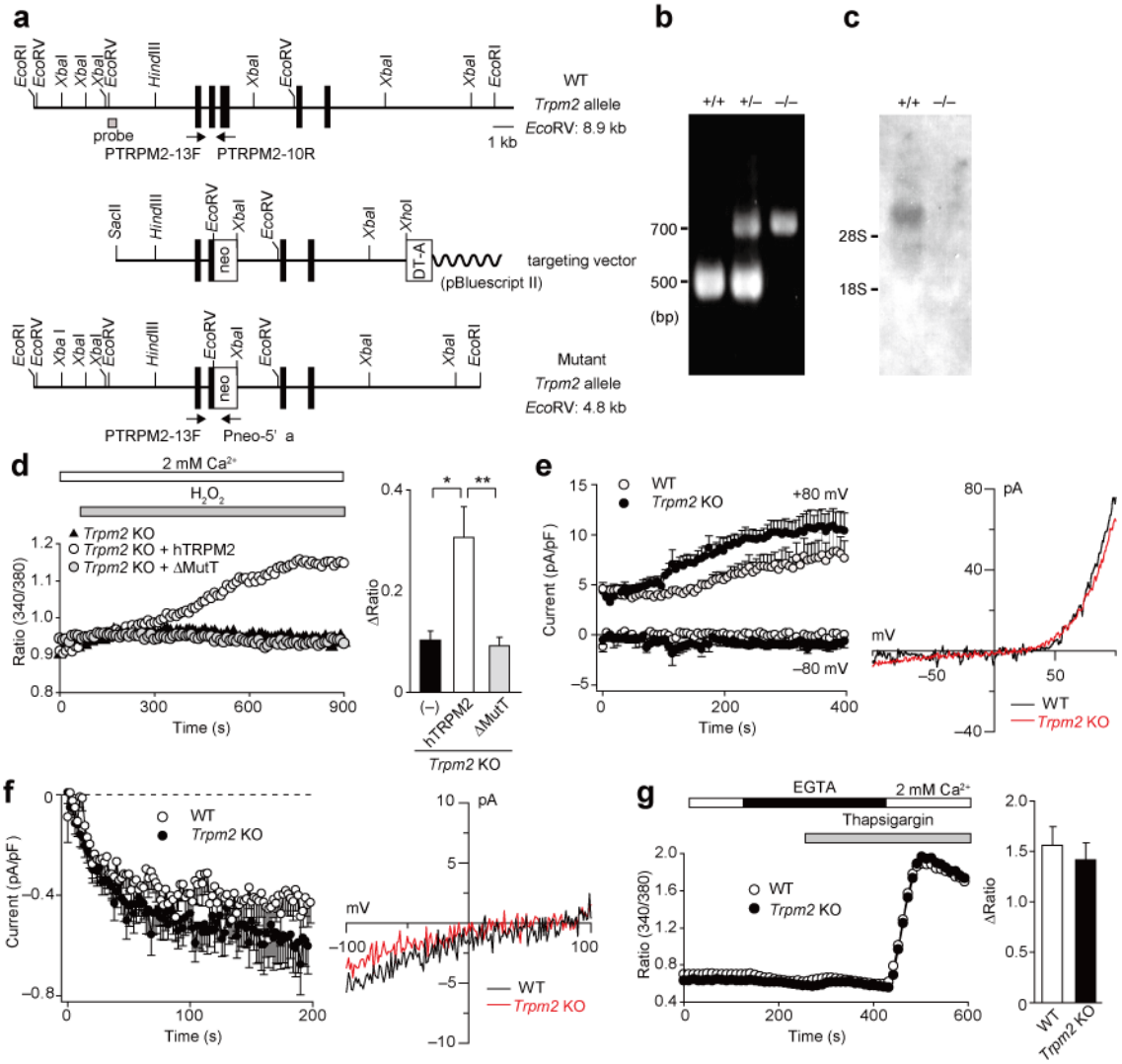

Supplementary Figure 3. Generation and characterization of *Trpm2* KO monocytes. (**a**) Restriction enzyme maps of the WT allele, targeting vector, and expected targeted allele. The exons in *Trpm2* allele (black box), neomycin resistance gene (neo), and diphtheria toxin (DT-A) are indicated. The genomic DNA probe used for Southern blot screening with *Eco*RV and PCR primers utilized for mouse genotyping (PTRPM2-13F, PTRPM2-10R, and Pneo-5'a) are shown. The nucleotide sequence encompassing the *Trpm2* allele has been deposited to the nucleotide databases with the accession number AC007433. (**b**) PCR analysis reveals disruption of the *Trpm2* gene in mouse genome. (**c**) Northern blot analysis of total RNA isolated from the brain reveals disruption of TRPM2 RNA expression in *Trpm2* KO mice. (**d**) H_2O_2-induced Ca^{2+} response after transfection with human TRPM2 (hTRPM2) or MutT-deleted hTRPM2 (ΔMutT) in *Trpm2* KO monocytes. Averaged time courses of $[Ca^{2+}]_i$ changes (left panel) and maximum $[Ca^{2+}]_i$ elevation (right panel) induced by 25 μM H_2O_2 in *Trpm2* KO monocytes transfected with hTRPM2 constructs (n = 15–30). (**e–g**) Intact Mg^{2+}/ATP-sensitive, TRPM7-like currents and I_{CRAC} in *Trpm2* KO monocytes. (**e**) Averaged development of Mg^{2+}/ATP-sensitive, TRPM7-like currents in WT (n = 5) and *Trpm2* KO monocytes (n = 5) (left panel). Data are acquired using a voltage ramp from –100 mV to +100 mV over 50 ms at a rate of 0.5 Hz. Current amplitudes are measured at –80 mV and 80 mV, normalized to cell size, averaged and plotted versus time of the experiment. Data are not leak subtracted. Representative I-V relationship of Mg^{2+}/ATP-sensitive, TRPM7-like current measured in WT or *Trpm2* KO monocyte (right panel). I-V data are leak corrected by subtracting the 3rd ramp recorded after whole-cell break-in from all ramps recorded per cell. (**f**) Averaged time course I_{CRAC} development measured in WT (n = 11) or *Trpm2* KO monocytes (n = 18) (left panel). The external solution contained (in mM): 10 $CaCl_2$, 140 NaCl, 2.8 KCl, 2 $MgCl_2$, 10 HEPES-NaOH. The internal solution contained (in mM): 120 Cs-glutamate, 3 $MgCl_2$, 8 NaCl, 10 HEPES-CsOH, 10 CsBapta, 0.02 inositol 1,4,5 trisphosphate. Data are leak-corrected by subtraction of the 2nd or 3rd ramp recorded after whole-cell break-in from all ramps recorded per cell. Averaged I-V curves of CRAC currents measured in WT (n = 3) or *Trpm2* KO monocytes (n = 5) (right panel). (**g**) Averaged time courses of $[Ca^{2+}]_i$ changes (left panel) and maximum $[Ca^{2+}]_i$ elevations (right panel) due to Ca^{2+} influx induced through store depletion by thapsigargin (2 μM) in monocytes isolated from peripheral blood of WT and *Trpm2* KO mice (n = 22–25). After 3 min exposure to 2 μM thapsigargin in Ca^{2+}-free, 0.5 mM EGTA-containing solution, cells are exposed to 2 μM thapsigargin and then to 2 mM Ca^{2+} to evoke Ca^{2+} response due to store-operated Ca^{2+} influx. Data points are mean ± s.e.m.. * $P < 0.05$ and ** $P < 0.01$.

Supplementary Figure 3

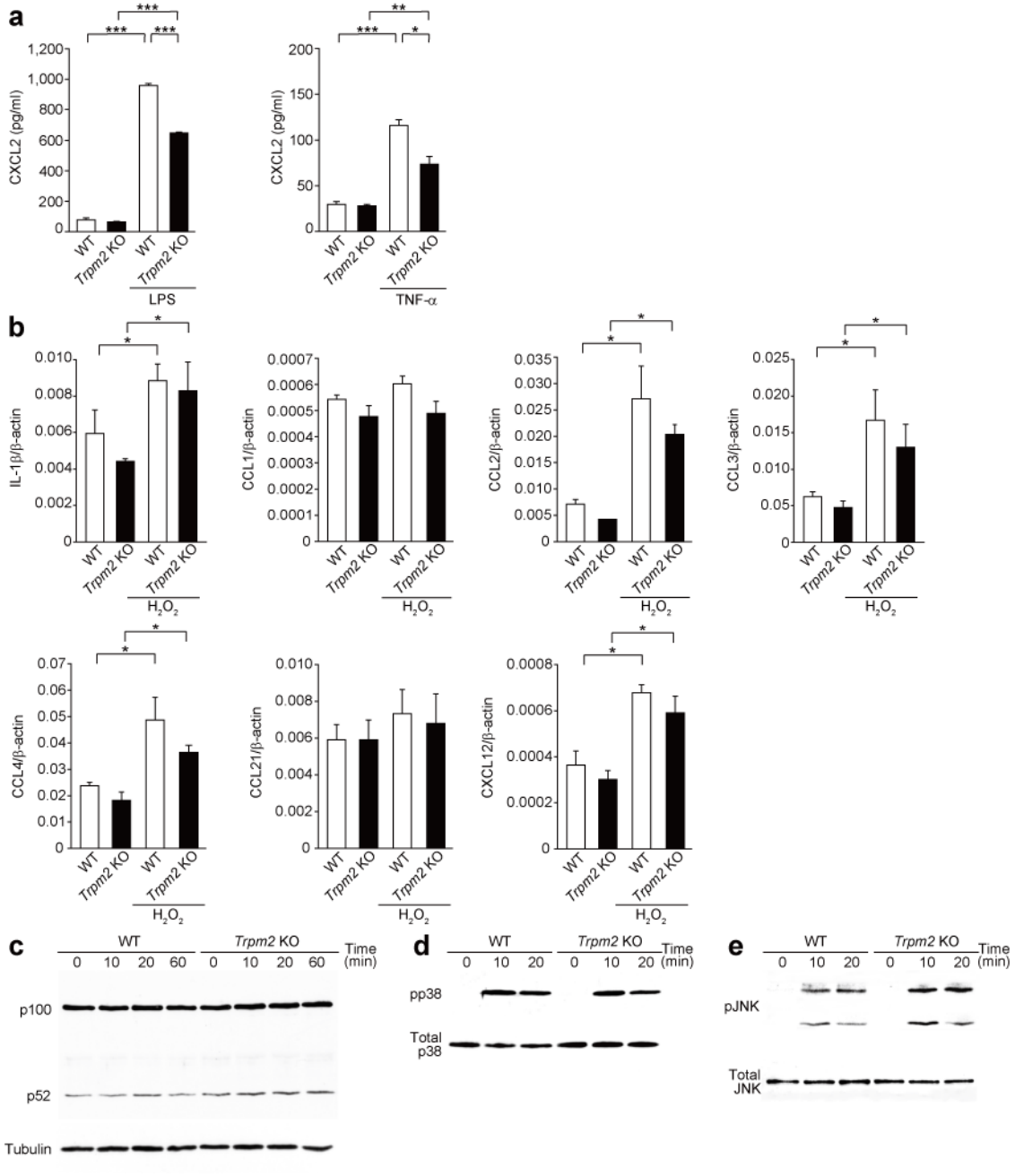

Supplementary Figure 4. H_2O_2-induced responses in isolated *Trpm2* KO monocytes. (**a**) CXCL2 production induced by LPS or TNF-α is diminished in *Trpm2* KO monocytes. CXCL2 secretion induced by incubation with 10 ng ml^{-1} LPS (left panel) or 10 ng ml^{-1} TNF-α (right panel) for 6 h is quantitated by ELISA. (**b**) Comparison of H_2O_2-induced cytokine and chemokine expression between WT and *Trpm2* KO monocytes. mRNA levels of IL-1β, CCL1, CCL2, CCL3, CCL4, CCL21, and CXCL12 are quantitated by real-time PCR after 3 h incubation with and without H_2O_2 (25 μM). Expression of CXCL1, CCL19, and CXCL13 was not detected in mouse monocytes. (**c**) H_2O_2 insensitivity of non-canonical NF-κB pathway in monocytes isolated from WT or *Trpm2* KO mice. Processing of the non-canonical NF-κB pathway protein p100 into p52 induced by incubation with 25 μM H_2O_2 is assessed at indicated time points by Western blot. (**d,e**) H_2O_2-induced p38-MAPK and JNK activation in monocytes isolated from WT or *Trpm2* KO mice. (**d**) p38-MAPK activation induced by 25 μM H_2O_2 at indicated time points of treatment. Activated p38-MAPK (pp38) is assessed by Western blot using phospho-p38-MAPK-specific antibody. (**e**) JNK activation induced by 25 μM H_2O_2 at indicated time points of treatment. Activated JNK (pJNK) is assessed by Western blot using phospho-JNK-specific antibody. Data points are mean ± s.e.m.. * $P < 0.05$, ** $P < 0.01$, and *** $P < 0.001$.

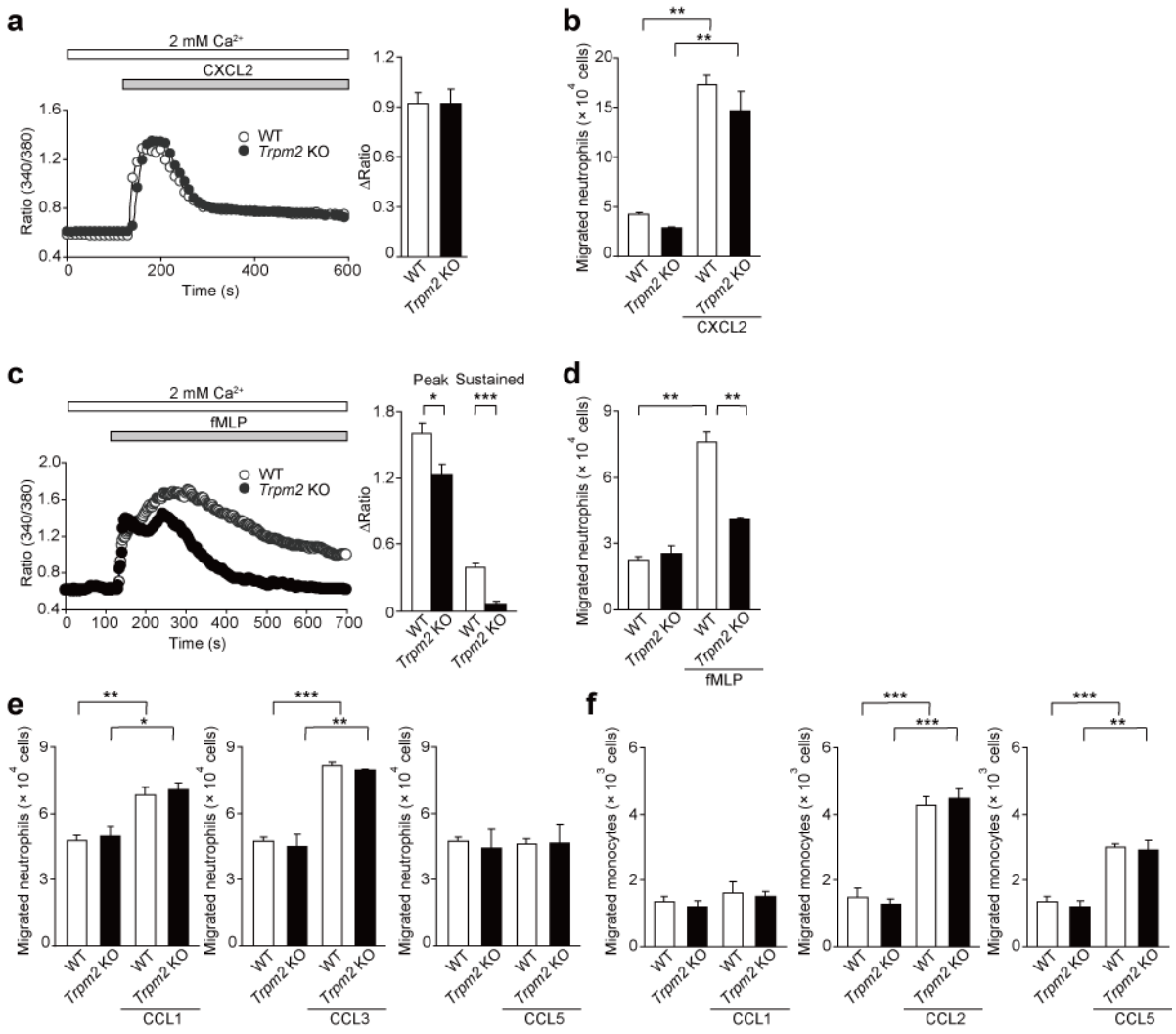

Supplementary Figure 5. *in vitro* chemotactic responses of neutrophils and monocytes from *Trpm2* KO mice. (**a**–**d**) *Trpm2* KO neutrophils show intact CXCL2-induced but impaired fMLP-induced functions. (**a**) Averaged time courses of $[Ca^{2+}]_i$ changes (left panel) and maximum $[Ca^{2+}]_i$ elevation (right panel) induced by CXCL2 (10 ng ml^{-1}) in neutrophils isolated from bone marrow of WT (n = 69) and *Trpm2* KO (n = 49) mice. (**b**) *in vitro* migration induced by CXCL2 (10 ng ml^{-1}) of neutrophils isolated from bone marrow of WT and *Trpm2* KO mice. The number of migrating cells is evaluated after cells are allowed to migrate to the lower chamber for 45 min. (**c**) Averaged time courses of $[Ca^{2+}]_i$ changes (left panel), and peak and sustained (after 10 min) $[Ca^{2+}]_i$ rises induced by fMLP (1 μM) (right panel) in neutrophils isolated from bone marrow of WT (n = 68) and *Trpm2* KO (n = 66) mice. (**d**) *in vitro* migration induced by fMLP (1 μM) of neutrophils isolated from bone marrow of WT and *Trpm2* KO mice. The number of migrating cells is evaluated after cells are allowed to migrate to the lower chamber for 45 min. (**e**,**f**) *in vitro* migration assays for neutrophils and monocytes. (**e**) *in vitro* migration induced by CCL1 (100 ng ml^{-1}), CCL3 (25 ng ml^{-1}), and CCL5 (100 ng ml^{-1}) of neutrophils isolated from bone marrow of WT and *Trpm2* KO mice. The number of migrating cells is assessed after cells are allowed to migrate to the lower chamber for 45 min. (**f**) *in vitro* migration induced by CCL1 (100 ng ml^{-1}), CCL2 (25 ng ml^{-1}), and CCL5 (100 ng ml^{-1}) of monocytes isolated from peripheral blood of WT and *Trpm2* KO mice. The number of migrating cells is assessed after cells are allowed to migrate to the lower chamber for 60 min. Data points are mean ± s.e.m.. * $P < 0.05$, ** $P < 0.01$, and *** $P < 0.001$.

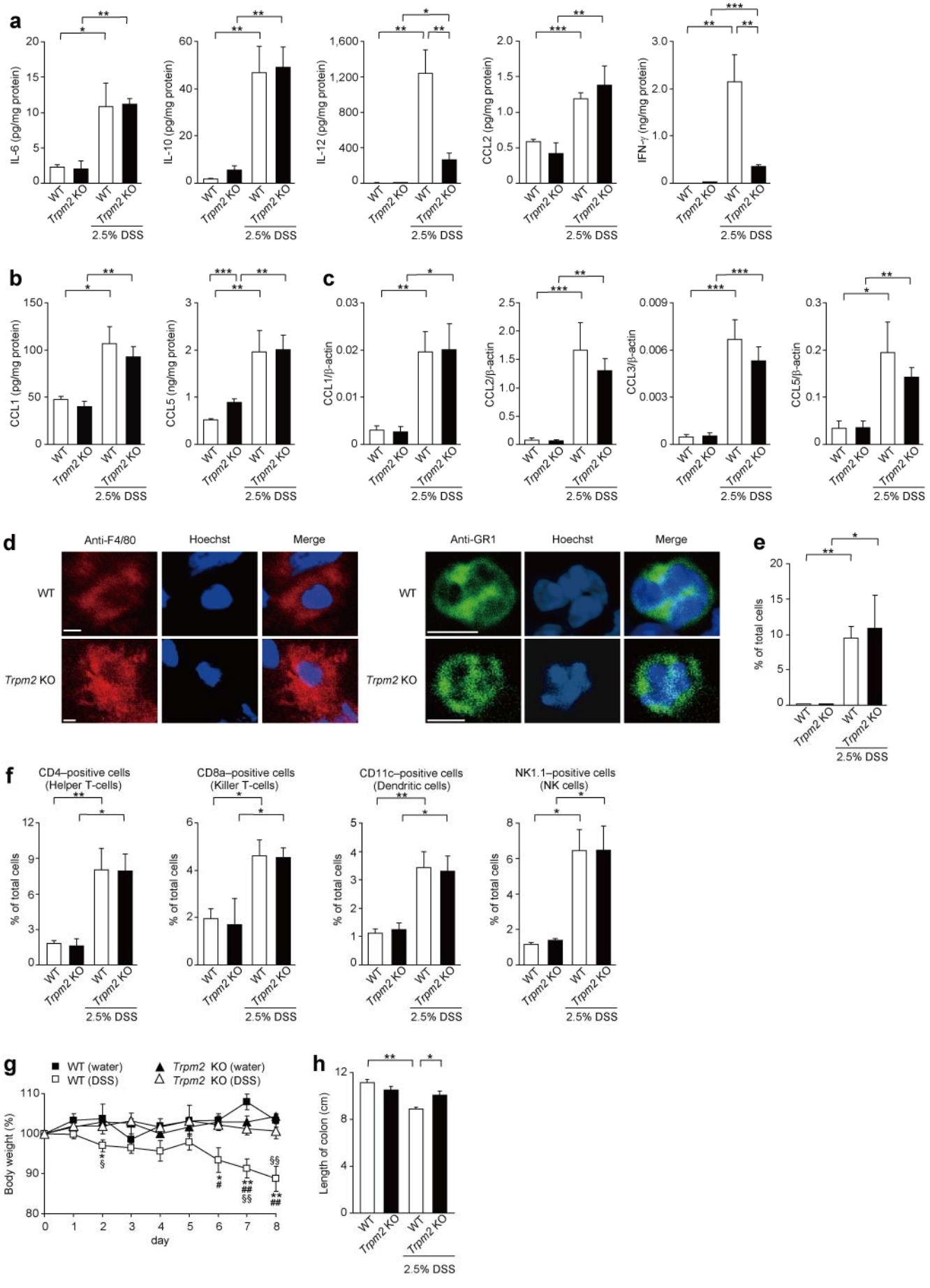

Supplementary Figure 6

Supplementary Figure 6. DSS-induced phenotypes in *Trpm2* KO mice. (**a–c**) Comparison of DSS-induced cytokine expression in the colon between WT and *Trpm2* KO mice. (**a**) Expression levels of IL-6, IL-10, IL-12, CCL2, and IFN-γ proteins determined using cytometric bead array. (**b**) Expression levels of CCL1 and CCL5 proteins determined using ELISA. (**c**) Expression levels of CCL1, CCL2, CCL3, and CCL5 mRNA quantitated by real-time PCR. Data points are mean ± s.e.m.. * $P < 0.05$, ** $P < 0.01$, and *** $P < 0.001$. (**d**) Fluorescent images of neutrophils or macrophages with nuclear stains in the colon of DSS-treated WT and *Trpm2* KO mice. R-PE-conjugated mouse F4/80-specific antibody (red) or FITC-conjugated mouse GR1-specific antibody (green) is used to aim at staining macrophages (left panel) or neutrophils (right panel), respectively. Nuclear staining with Hoechst 33342 reveals that F4/80-positive cells show a round nucleus observed for macrophages but GR1-positive cells multilobulated nucleus observed for neutrophils. The bars indicate 5 μm. (**e**) Infiltration of $CD11b^{+}Ly6C^{high}Ly6G^{low}$ macrophages into the colon of DSS-treated mice. $CD11b^{+}Ly6C^{high}Ly6G^{low}$ macrophages dissociated from the WT and *Trpm2* KO colon are counted with flow cytometer using antibodies to antigens CD11b, Ly6C, and Ly6G. Data points are mean ± s.e.m.. * $P < 0.05$ and ** $P < 0.01$. (**f**) Infiltration of other immunocytes into the colon of DSS-treated mice. Helper T-cells, killer T-cells, dendritic cells, and NK cells dissociated from the WT and *Trpm2* KO colon are counted with flow cytometer using antibodies to antigens CD4, CD8a, CD11c, and NK1.1, respectively. Data points are mean ± s.e.m.. * $P < 0.05$ and ** $P < 0.01$. (**g,h**) *Trpm2* KO mouse is resistant to DSS-induced body weight loss and colon shortening. (**g**) Time courses of 2.5% DSS-induced body weight loss. WT or *Trpm2* KO mice are treated with water or DSS for indicated periods, and body weight is measured daily. Relative body weight (%) on each day compared with that of day 0 is plotted. Data points are mean ± s.e.m.. * $P < 0.05$ and ** $P < 0.01$ versus DSS-treated *Trpm2* KO group, # $P < 0.05$, ## $P < 0.01$ versus water-treated WT group, and § $P < 0.05$, § § $P < 0.01$ versus water-treated *Trpm2* KO group. (**h**) The length of the colons in each group is depicted. Colons are obtained on day 8 from each group. Data points are mean ± s.e.m.. * $P < 0.05$ and ** $P < 0.01$.

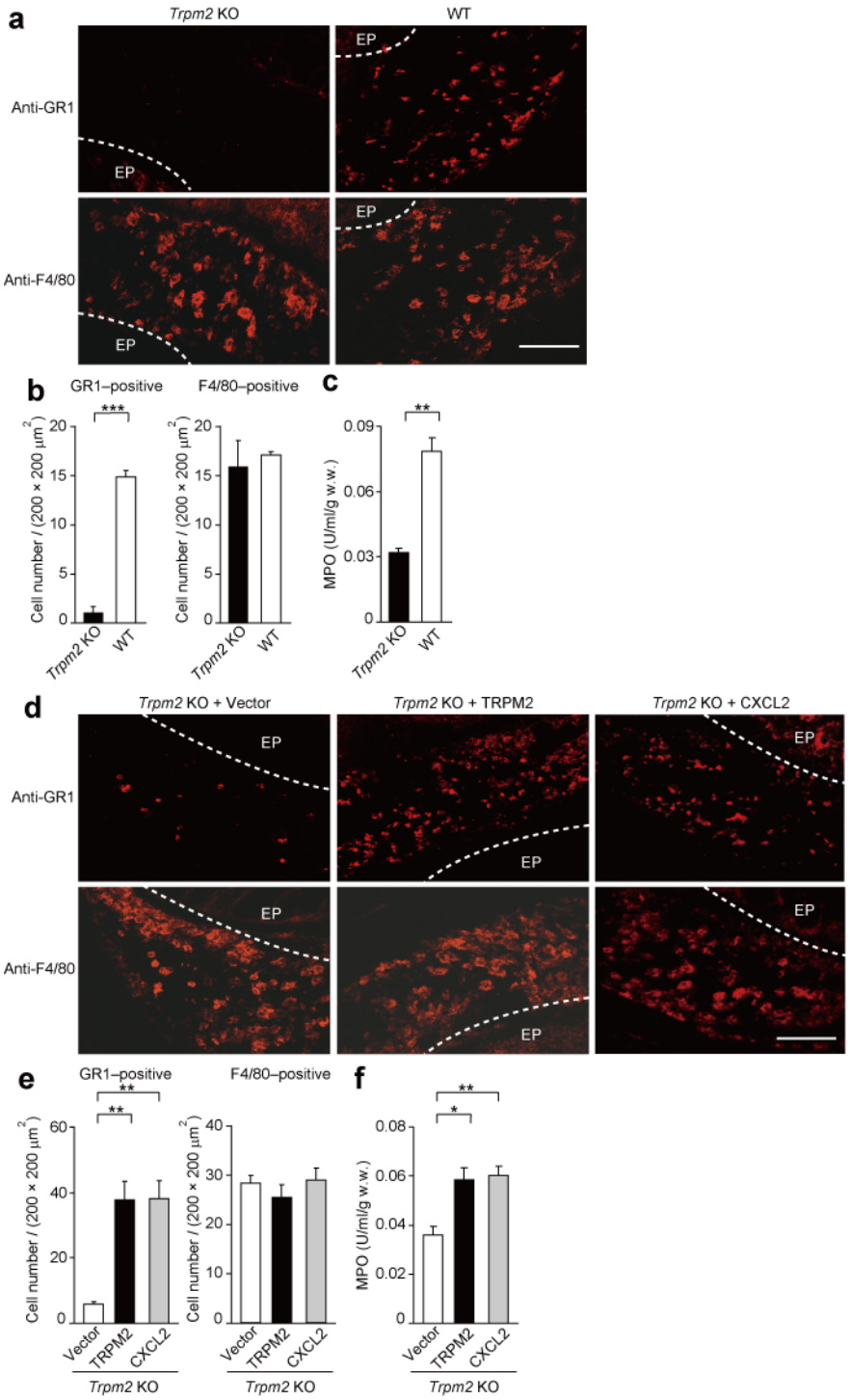

Supplementary Figure 7. Transfer of WT, TRPM2-infected, and CXCL2-infected bone marrow-derived macrophages accumulates neutrophils in the colon of DSS-treated *Trpm2* KO mice. (**a**) Immunofluorescent staining of colon tissue is performed with R-PE-conjugated mouse GR1-specific antibody (upper panels) and R-PE-conjugated mouse F4/80-specific antibody (lower pannel). Bone marrow-derived macrophages (BMDMs) are injected into the tail vein of *Trpm2* KO mice administered with 2.5% DSS for 6 days. GR1-positive cell (neutrophil) infiltration is restored by WT BMDMs but not by *Trpm2* KO BMDMs. The bar indicates 100 μm. EP, epithelium. (**b**) GR1-positive cells (left) and F4/80-positive cells (right) in the colon of *Trpm2* KO mice transferred with WT and *Trpm2* KO BMDMs are counted. (**c**) Activity of MPO in the colon of *Trpm2* KO mice transferred with WT and *Trpm2* KO BMDMs. (**d**) GR1-positive cell infiltration is restored by *Trpm2* KO BMDMs infected with TRPM2 or CXCL2 cDNA-containing retroviruses but not by *Trpm2* KO BMDMs infected with empty viruses in the colon of *Trpm2* KO mice. (upper panels) GR1-positive cells. (lower pannel) F4/80-positive cells. (**e**) GR1-positive cells (left) and F4/80-positive cells (right) in the colon of *Trpm2* KO mice transferred with virus-infected *Trpm2* KO BMDMs are counted. (**f**) Activity of MPO in the colon of *Trpm2* KO mice transferred with virus-infected *Trpm2* KO BMDMs. Data points are mean ± s.e.m.. * $P < 0.05$, ** $P < 0.01$, and *** $P < 0.001$.

Supplementary Figure 7

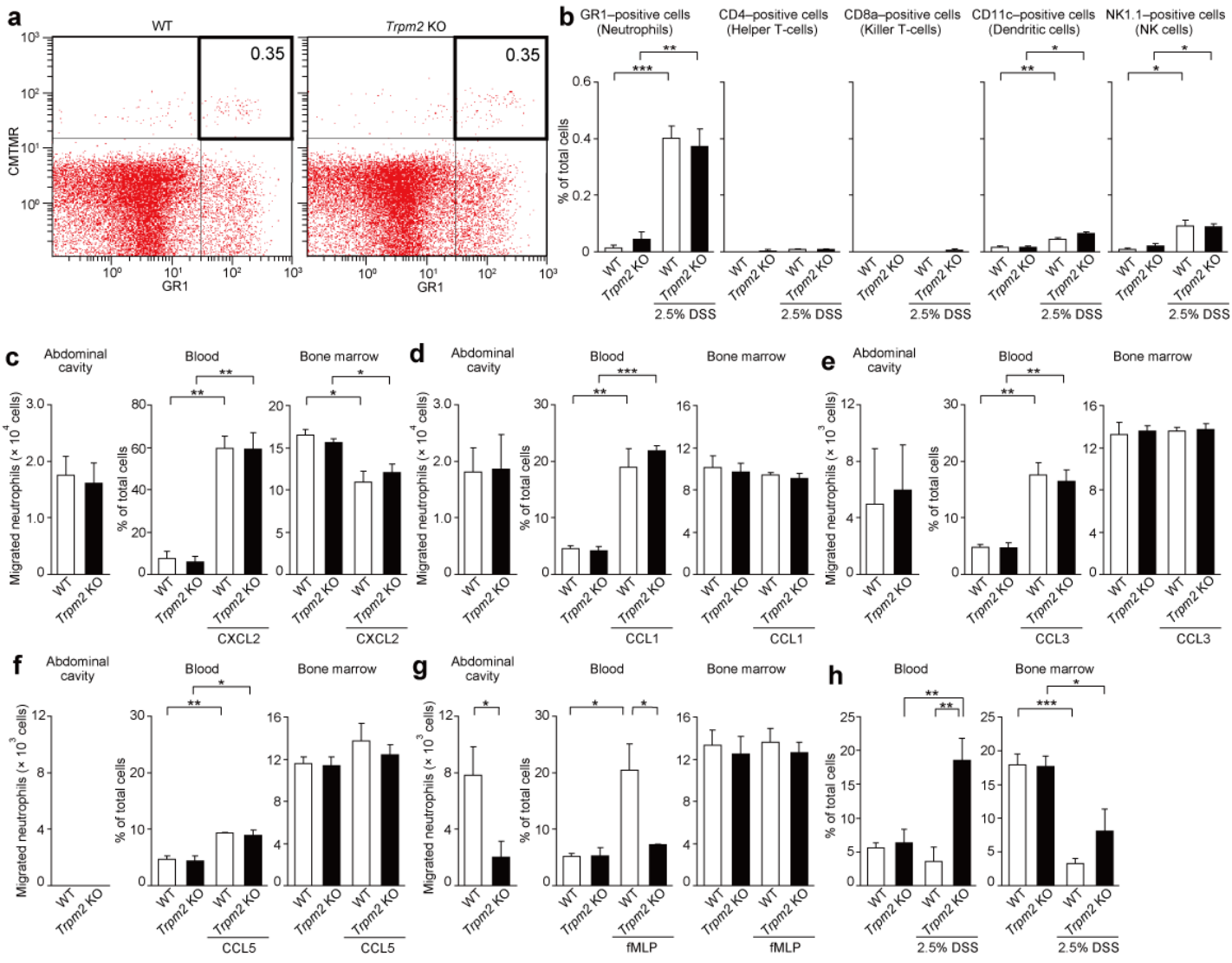

Supplementary Figure 8. *in vivo* neutrophil chemotaxis in mice. (**a**) *in vivo* migration of WT and *Trpm2* KO neutrophils in the DSS model mice. Flow cytometric analyses are carried out for CMTMR-labeled WT and *Trpm2* KO cells infiltrated to the colon after bone marrow transfer in DSS-treated WT mice. Bone marrow cells isolated from WT or *Trpm2* KO mice are labeled with CMTMR, and transferred by intravenous injection into the tail veins of WT mice administered with 2.5% DSS for 7 days. Next day, the colon is collected and CMTMR-labeled cells are quantified by flow cytometer. Representative flow cytometry histograms indicate CMTMR-labeled, GR1-positive WT or *Trpm2* KO neutrophils migrated to the colon are 0.35% among the live cells gated. The averaged value for ratios between infilterated neutrophils in the pair of DSS-treated WT mice transferred with WT or *Trpm2* KO bone marrow cells is 0.96 ± 0.11 (5 sets of experiment are performed). GR1-positive WT and *Trpm2* KO neutrophils have equivalent ability of migration in response to chemoattractants release from the colon. (**b**) CMTMR-labeled WT and *Trpm2* KO immunocytes infiltrated to the colon after bone marrow transfer in DSS-treated WT mice. CMTMR-labeled helper T-cells, killer T-cells, dendritic cells, and NK cells dissociated from the WT and *Trpm2* KO colon are counted with flow cytometer using antibodies to antigens CD4, CD8a, CD11c, and NK1.1, respectively. (**c–g**) Neutrophil migration induced by intraperitoneal injection of CXCL2, CCL1, CCL3, CCL5, or fMLP. CXCL2 (1.0 μg) (**c**), CCL1 (2.5 μg) (**d**), CCL3 (1.0 μg) (**e**), CCL5 (2.5 μg) (**f**), and fMLP (10 nmol) (**g**) in 500 μl PBS or PBS as control is intraperitoneally injected into WT and *Trpm2* KO mice. After 30 min, the number of neutrophils infiltrated into the abdominal cavity (left panel) and the neutrophil contents of blood (middle panel) and bone marrow (right panel) are measured. The number of migrated neutrophils is determined by subtracting neutrophil number in PBS-treated mice from that in chemokine-treated mice. Neutrophil infiltrated into the abdominal cavity toward injected CCL5 is absent. Helper T-cells show similar CCL5-induced abdominal infiltration in WT and *Trpm2* KO mice (15.0 ± 0.11 and 14.7 ± 0.15 (× 10^4 cells), respectively). (**h**) Bone marrow output of neutrophils elicted by DSS treatment in WT and *Trpm2* KO mice. Neutrophil contents of blood and bone marrow are measured by flow cytometer. The content of neutrophils circulating in the blood of WT DSS model is indistinguishable with that of the untreated control, which can be attributable to an efficient infiltration of neutrophils to the colon (Rijcken *et al. Am. J. Physiol. Gastrointesto. Liver Physiol.* 293, 446–452 (2007)) or to a loss of neutrophils through bloody bowel discharge (Niren *et al. J. Trauma* 45, 7–13 (1998)). Data points are mean ± s.e.m.. * $P < 0.05$, ** $P < 0.01$, and *** $P < 0.001$.

Supplementary Figure 8

SUPPLEMENTARY METHODS

Cell culture. The human monocytotic cell line U937 was routinely cultured in RPMI 1640 medium supplemented with 10% fetal bovine serum, 30 units ml^{-1} penicillin, and 30 mg ml^{-1} streptomycin at 37 °C under 5% CO_2.

Isolation of mouse monocytes. Peripheral blood was collected from abdominal aorta of mouse. The collected blood was separated by using Nycoprep 1.077 A (AXIS-SHIELD) to obtain peripheral blood mononuclear cells (PBMC). Monocytes were isolated from the PBMC by CD11b positivity using a magnetic activated cell sorting system (Miltenyi Biotech). All animal experiments were performed in accordance with protocols approved by the Institutional Animal Care and Use Committees of the Graduate School of Engineering, Kyoto University.

Northern blot analysis. RNA from each sample was treated with the solution containing 2.2 M formaldehyde, 50% formamide, 5 mM sodium acetate, 1 mM EDTA, and 20 mM 3-morpholinopropanesulfonic acid (MOPS, pH 7.0) for 15 min at 65 °C. The RNA was separated by electrophoresis through 1% agarose gel containing 5 mM sodium acetate, 1 mM EDTA, and 20 mM MOPS (pH 7.0), transferred to Hybond-N nylon membranes (Amersham Pharmacia Biotech), and hybridized with ^{32}P-labeled, random-primed cDNA probe. The cDNA probe templates of TRPM2, CXCL8, and 18S rRNA were prepared by RT-PCR using specific primers 5'-CTACAGTGCCCCTTCGGCAA-3' (sense) and 5'-TCTGAGCCAAATTGACCAGG-3' (anti-sense) for TRPM2,

5’-CTGATTTCTGCAGCTCTGTG-3’ (sense) and 5’-TTCACTGGCATCTTCACTG-3’ (anti-sense) for CXCL8, and 5’-GAAAGTCGGAGGTTCGAAGA-3’ (sense) and 5’-ACCAACTAAGAACGGCCATG-3’ (anti-sense) for 18S rRNA. Hybridization reaction was carried out for 1 h at 68 °C in ExpressHyb hybridization solution (Clontech). The membrane was washed for 15 min at room temperature with 2 × SSC containing 0.05% SDS twice, and for 15 min with 0.1 × SSC containing 0.1% SDS at 55 °C twice. The washed membrane was exposed to Kodak Biomax film at –80 °C for 24–48 h.

RT-PCR. Expression levels of CXCL8, CCL23, IKK-β, IκB-α, RelA, p105, RasGRP2, RasGRP4, and GAPDH mRNA in the U937 cells were determined by RT-PCR using specific primers 5’-CTGATTTCTGCAGCTCTGTG-3’ (sense) and 5’-TTCACTGGCATCTTCACTG-3’ (anti-sense) for CXCL8, 5’-CGAGAAGCCAGGAAGCAGTG-3’ (sense) and 5’-TTGGAGCACTCGCTGTTCG-3’ (anti-sense) for CCL23, 5’-GAGAACGAAGTGAAACTCCTGGTAGAACGG-3’ (sense) and 5’-GCTGGCTCAGGTAAGCTGTTGGAGG-3’ (anti-sense) for IKK-β, 5’-GACGAGGAGTACGAGCAGATGGTCAAG-3’ (sense) and 5’-GACACGTGTGGCCATTGTAGTTGGTAG-3’ (anti-sense) for IκB-α, 5’-ACCTCGACGCATTGCTGTGCCTTCC-3’ (sense) and 5’-GTCCATGTCCGCAATGGAGGAGAAGTC-3’ (anti-sense) for RelA, 5’-GGAAGATGTGGTGGAGGATTTGCTGAGGG-3’ (sense) and 5’-GCTTTGAGAAGAGCTGCCAGCCTGGTG-3’ (anti-sense) for p105, 5’-TACCTCAGCGCCTTTGGGGACCTC-3’ (sense) and

5’-CAGAGAGAAGCTGAAGGCGCGGTG-3’ (anti-sense) for RasGRP2, 5’-CCACGCCAGGGGAGAGGATCCTTC-3’ (sense) and 5’-TCCTGCATCGCCCTTGGCCCCTGG-3’ (anti-sense) for RasGRP4, and 5’-CAGGGCTGCTTTTAACTCTG-3’ (sense) and 5’-GATGATCTTGAGGCTGTTGTC-3’ (anti-sense) for GAPDH. Temperature cycles were as follows: 94 °C for 1 min followed by 28 cycles at 94 °C for 30 s, 60 °C for 30 s, 72 °C for 35 s for CXCL8 and RasGRP4, 22 cycles at 94 °C for 30 s, 58 °C for 30 s, 72 °C for 35 s for CCL23, 30 cycles at 94 °C for 30 s, 62 °C for 30 s, 72 °C for 35 s for IKK-β and IκB-α, 30 cycles at 94 °C for 30 s, 65 °C for 30 s, 72 °C for 40 s for RelA and p105, 24 cycles at 94 °C for 30 s, 60 °C for 30 s, 72 °C for 35 s for RasGRP2, and 20 cycles at 94 °C for 30 s, 55 °C for 30 s, 72 °C for 35 s for GAPDH.

Small interfering RNA. The TRPM2 siRNA sequence targeting the coding region of TRPM2 mRNA (5’-AAAGCCTCAGTTCGTGGATTC-3’) was used. The Pyk2 siRNA sequences targeting the coding region of Pyk2 mRNA (5’-AATGCACTTGACAAGAAGTCC-3’), (5’-AAGATGTGGTCCTGAATCGTA-3’), (5’-AAGGTGTCTACACAAATCACA-3’), and (5’-AAGTCCCTGGACCCCATGGTT-3’) were used. The RasGRP2 and RasGRP4 siRNA sequence targeting the coding region of RasGRP2 mRNA (5’-AAGGCTCTGCTAGACCAAGAA-3’) and RasGRP4 mRNA (5’-AAGACGAGATCTATGAGCTTT-3’) were used, respectively. The siRNA duplex was synthesized and purified using the Silencer siRNA Construction Kit (Ambion) according to the manufacturer’s protocol. After 48 h of siRNA transfection, cells were used for experiments. During the 48 h period, the serum concentration was reduced

from 10% to 2.5%, in order to prevent siRNAs from dilution through vigorous cellular proliferation. A siRNA directed against glyceraldehyde-3-phosphate dehydrogenase (GAPDH) provided in the kit was used as a control.

Transfection. Transfections of siRNAs or Pyk2-DN into U937, and hTRPM2 or MutT-deleted hTRPM2[1] into monocytes isolated from peripheral blood of *Trpm2* KO mice were performed by using Nucleofector, a system consisting of an electroporation device and a solution to suspend cells (Amaxa) according to the manufacturer's protocol.

Western blot analysis. Activation of Erk, Pyk2, IκB, IKK-β/IKK-α, p38-MAPK, and JNK were determined by Western blot with phospho-Erk1/2-specific antibody (Cell Signaling), phospho-Pyk2-specific antibody (Biosource), phospho-IκB-specific antibody (Cell Signaling), phospho-IKK-β/IKK-α-specific antibody (Cell Signaling), phospho-p38-MAPK-specific antibody (Cell Signaling), and phospho-JNK-specific antibody (Cell Signaling), respectively using the ECL system (Amersham Pharmacia Biotech). Degradation of IκB was also determined by Western blot with IκB-specific antibody (Santa Cruz Biotech). Cells were lysed in lysis buffer (50 mM Tris-HCl pH 7.5, 150 mM NaCl, 5 mM EDTA, 1% Triton X-100, 0.1 mM sodium orthovanadate, 2 mM dithiothreitol, 2 mM phenylmethylsulfonyl fluoride, 10 μg ml^{-1} leupeptin, and 5 μg ml^{-1} aprotinin) for 10 min on ice. After centrifugation at 15,000 rpm for 10 min, lysates were subjected to 10% SDS-PAGE and electrotransferred onto a nitrocellulose membrane. The total amount of Erk2, Pyk2, IKK-α, IKK-β, tubulin, p38-MAPK, and JNK were detected by using Erk2-specific antibody (Santa Cruz Biotech), Pyk2-specific

antibody (Upstate), IKK-α-specific antibody (Cell Signaling), IKK-β-specific antibody (Cell Signaling), tubulin-specific antibody (Sigma), p38-MAPK-specific antibody (Cell Signaling), and JNK-specific antibody (Cell Signaling), respectively. Processing of p100 into p52 was also determined by Western blot with NF-κB2 p100-specific antibody (Cell Signaling).

Ras-GTP assay. Ras-GTP assay was performed as described previously[2]. In brief, bacterially expressed GST-Ras binding domain (amino acids 1–149 of human cRaf-1 fused to GST) prebounded glutathione-Sepharose beads (Amersham Pharmacia Biotech) was prepared. Each cell lysate in Mg^{2+}-containing lysis buffer was incubated with the beads for 15 min at 4 °C. After washing 3 times with Mg^{2+}-containing lysis buffer, bound proteins were eluted with SDS-PAGE sample buffer and resolved on 15% SDS-PAGE and subjected to Western blot with pan-Ras-specific antibody (Calbiochem).

Nuclear translocation of NF-κB. Nuclear translocation of the canonical or non-canonical NF-κB protein was determined by Western blot with RelA-specific antibody (Santa Cruz Biotech) or NF-κB2 p100-specific antibody (Cell Signaling), respectively. Cells were washed once with PBS and resuspended in buffer A (10 mM HEPES-KOH (pH 7.8), 10 mM KCl, 0.1 mM EDTA, 0.1% NP40, 1 mM DTT, 0.1 mM sodium orthovanadate, 0.5 mM PMSF, 2 μg ml^{-1} aprotinin, and 2 μg ml^{-1} leupeptin) for 5 min on ice. After centrifugation at 5,000 rpm for 2 min, the nuclear pellet was resuspended in buffer B (50 mM HEPES-KOH (pH 7.8), 420 mM KCl, 0.1 mM EDTA, 5 mM $MgCl_2$, 1 mM DTT, 0.1 mM sodium orthovanadate, 0.5 mM PMSF, 2 μg ml^{-1}

aprotinin, and 2 μg ml^{-1} leupeptin) and incubated for 30 min on ice. After centrifugation at 15,000 rpm for 15 min, lysates were subjected to 10% SDS-PAGE and electrotransferred onto a nitrocellulose membrane. The total amount of β-actin was detected by using β-actin-specific antibody (Sigma) as the loading control.

NF-κB activity. NF-κB activation was measured with the EZ-Detect NF-κB p65 Transcription Factor Kit (Pierce) according to the manufacturer's instructions.

Pyk2 dominant negative form. The dominant-negative mutant of $Pyk2^{K457A}$ was generated by replacing lysine 457 with alanine using PCR techniques[3]. The mutation was confirmed by sequence analysis.

Immunoprecipitation. Cells were lysed in ice-cold RIPA buffer (50 mM Tris (pH 8.0), 150 mM NaCl, 1% NP-40, 0.5% sodium deoxycholate, 0.1% SDS, 1 mM PMSF, 1 mM sodium orthovanadate, 25 mM NaF, 10 μg ml^{-1} aprotinin, and 10 μg ml^{-1} leupeptin). Lysates were clarified by centrifugation at 15,000 rpm for 10 min. The lysates were immunoprecipitated for 2 h at 4 °C with protein A-agarose linked to Pyk2-specific antibody (Upstate). Immunoprecipitates were washed 3 times with RIPA buffer and resuspended in SDS sample buffer. The protein samples were fractionated by 7.5% SDS-PAGE and electrotransferred onto a nitrocellulose membrane. The blots were incubated with phosphotyrosine-specific antibody (Upstate).

Generation of *Trpm2* KO mice. The *Trpm2* gene was disrupted by deleting the exon encoding the transmembrane segment 5 and part of the linker between segments 5 and 6,

which has been suggested to contribute to the pore forming region of the Trpm2 protein[4] (**Supplementary Fig. 3a**). A 129/SvJ mouse genomic library (Stratagene) was screened by hybridization with a 2.2 kb *Eco*RI fragment of pmLTRPC2-1[1]. Three fragments containing the putative pore region of TRPM2 were obtained. The targeting vector was constructed with the obtained *Trpm2* genomic DNA, the neomycin resistance gene from pMC1 Neo polyA, the diphtheria toxin gene from pMC1-DT-A, and pBluescript II SK(–). In Southern blot screening, among the J1 ES cells[5] transfected with the vector, several clones carrying the expected homologous mutation were isolated (data not shown). Chimeric mice produced with the ES clones were crossed with C57BL/6J mice and could transmit the mutant gene to the pups. To determine the mouse genotype, PCR with the primer sets of PTRPM2-13F, PTRPM2-10R, and Pneo-5'a was carried out using genomic DNA from mice (**Supplementary Fig. 3b**); sequences are PTRPM2-13F (5'-CTTGGGTTGCAGTCATATGCAGGC-3'), PTRPM2-10R (5'-GCCCTCACCATCCGCTTCACGATG-3'), and Pneo5'a (5'-GCCACACGCGTCACCTTAATATGCG-3'). Northern blot analysis (**Supplementary Fig. 3c**) was performed as described previously[1]. Mice were kept in essentially specific pathogen-free environment, and analyses were performed using mice matched of gender and age.

Electrophysiology. Patch-clamp experiments were performed in the whole-cell configuration. Cells were kept in standard Ringer's solution (in mM): 140 NaCl, 2.8 KCl, 1 $CaCl_2$, 2 $MgCl_2$, 10 glucose, 10 HEPES-NaOH (pH 7.2 adjusted with NaOH). Standard pipette-filling solutions contained (in mM): 140 Cs-glutamate, 8 NaCl, 1

$MgCl_2$, 10 HEPES-CsOH (pH 7.2 adjusted with CsOH). Ca^{2+} was left unbuffered by leaving out any calcium chelator. ADPR or H_2O_2 was added to its final concentrations as appropriate. All data were acquired with 'Pulse' software controlling an EPC-9 amplifier (HEKA) and analyzed using FitMaster (HEKA) and Igor Pro (Wavemetrics). Voltage ramps of 50 ms duration spanning the voltage range from –100 to +100 mV were delivered from a holding potential of 0 mV at a rate of 0.5 Hz over a period of 200–500 s. Voltages were corrected for liquid junction potentials (10 mV). Currents were filtered at 2.9 kHz and digitized at 100 μs intervals. Capacitive currents and series resistance were determined and corrected before each voltage ramp. The ramp current amplitudes at –80 mV (inward current) were extracted from individual ramp data and displayed as current development over time. Some individual ramps were displayed as representative I-V relationships. Mg^{2+}/ATP-regulated TRPM7-like current and Ca^{2+}-release activated Ca^{2+} current (I_{CRAC}) were measured as previously reported[6,7].

Real-time PCR. Total RNA was extracted using ISOGEN (NIPPON GENE). Reverse-transcription of RNA to cDNA was performed using RNA LA PCR Kit (TaKaRa). Quantification was performed by real-time PCR (LightCycler Instrument, Roche) using the LightCycler FastStart DNA Master HybProbe Kit (Roche). The oligonucleotide primers used for CCL1 were 5’-CGTGTGGATACAGGATGTTGACAG-3’ (sense) and 5’-AGGAGGAGCCCATCTTTCTGTAAC-3’ (anti-sense), for CCL2 were 5’-TAGGCTGGAGAGCTACAAGAGG-3’ (sense) and 5’-AGTGCTTGAGGTGGTTGTGG-3’ (anti-sense), for CCL3 were

5’-CAGCGAGTACCAGTCCCTTTT-3’ (sense) and 5’-CCTCGCTGCCTCCAAGA-3’ (anti-sense), for CCL4 were 5’-GTTCTCAGCACCAATGGGCTCTGA-3’ (sense) and 5’-CTCTCCTGAAGTGGCTCCTCCTG-3’ (anti-sense), for CCL5 were 5’-ACGAGTCGATCTCCCACAGCCTCTGC-3’ (sense) and 5’-AAGCTGGCTAGGACTAGAGCAAGCGATGAC-3’ (anti-sense), for CCL21 were 5’-CTCTGAGCCTCCTTAGCCTGGTCCTG-3’ (sense) and 5’-GGCGGGCTACTGGGCTATCCTCTTG-3’ (anti-sense), for CXCL2 were 5’-GAACAAAGGCAAGGCTAACTG-3’ (sense) and 5’-AACATAACAACATCTGGGCAAT-3’ (anti-sense), for CXCL12 were 5’-CCAGTCAGCCTGAGCTACCG-3’ (sense) and 5’-CGGGTCAATGCACACTTGTC-3’ (anti-sense), for IL-1β were 5’-ATGGCAACTGTTCCTGAACTCAACT-3’ (sense) and 5’-CAGGACAGGTATAGATTCTTTCCTTT-3’ (anti-sense), and for β-actin were 5’-GATGACGATATCGCTGCGCTG-3’ (sense) and 5’-GTACGACCAGAGGCATACAGG-3’ (anti-sense). Temperature cycles were as follows: 95 °C for 10 min followed by 40 cycles at 95 °C for 10 s, 61 °C for 5 s, 72 °C for 10 s for CCL1, at 95 °C for 10 s, 62 °C for 5 s, 72 °C for 10 s, 86 °C for 10 s for CCL2, at 95 °C for 10 s, 60 °C for 10 s, 72 °C for 30 s, 86 °C for 10 s for CCL3, at 95 °C for 15 s, 60 °C for 5 s, 72 °C for 7 s for CCL4 and CXCL12, at 95 °C for 10 s, 64 °C for 5 s, 72 °C for 10 s for CCL5, at 95 °C for 10 s, 65 °C for 5 s, 72 °C for 10 s, 86 °C for 10 s for CCL21, at 95 °C for 10 s, 59 °C for 10 s, 72 °C for 30 s for CXCL2, at 95 °C for 10 s, 58 °C for 10 s, 72 °C for 20 s for IL-1β and at 95 °C for 10 s, 55 °C for 10 s, 72 °C for 30 s for β-actin. The results were analyzed with LightCycler software. The identity of the PCR product was confirmed by automated determination

of the melting temperature of the PCR products. The results for each gene were normalized relative to β-actin expression measured in parallel in each sample.

Isolation of bone marrow neutrophils. Mouse bone marrow neutrophils were isolated from femurs and tibias. Bone marrow cells were pelleted by centrifugation and suspended in 3 ml of a 45% Percoll (GE Healthcare). Two ml each of the 62, 55, and 50% Percoll solutions was layered successively onto 3 ml of the 81% solution. Finally, cells in 45% Percoll were layered on top of the gradient. After centrifugation at 1600 × *g* for 30 min, the neutrophil fraction between the 81 and 62% layer was collected. Remaining erythrocytes were lysed with the buffer containing (in mM): 150 NH_4Cl, 1 $KHCO_3$, and 0.1 Na_2EDTA.

in vitro **migration assay of neutrophils and monocytes stimulated with chemoattractants.** 6.5 mm diameter well chambers with 3 μm pore size membranes for neutrophils or 5 μm pore size membranes for monocytes (Costar) were used to determine chemotaxis. The medium containing CXCL2, fMLP, CCL1, CCL2, CCL3, and CCL5 were added to the lower chamber. Neutrophils (5×10^5 cells) or monocytes (1.5×10^5 cells) were allowed to migrate from the upper to lower chamber for 45 min and 1 h, respectively, and the number of migrating cells was counted.

Cytokines analysis by cytometric bead array (CBA). After 8 days of 2.5% DSS administration, whole colons were extirpated and lyzed with lysis buffer (100 mM Tris-HCl (pH7.8), 66 mM EDTA, 1% NP-40, 0.4% sodium deoxycholate, 1 mM PMSF). And then they were centrifuged for eliminating cells and debris. IL-6, IL-10, CCL2,

IFN-γ, and IL-12 were detected simultaneously using the mouse inflammation cytometric bead array (CBA) kit (BD Bioscience). All of manipulations were done in accordance with the manufacturers' instructions mentioned below. Fifty μl of each sample was mixed with 50 μl mixed capture beads and 50 μl mouse inflammation PE detection reagent consisting of PE-conjugated mouse IL-6-, IL-10-, CCL2-, IFN-γ-, and IL-12-specific antibody. The samples were incubated at room temperature for 3 h in the dark. After incubation with the PE detection reagent, the samples were washed once and re-suspended in 300 μL of wash buffer before acquisition on the EPICS ELITE XL. Data were analyzed using CBA software (BD Bioscience). Standard curves were generated for each cytokine using the mixed cytokine standard provided by the kit. The concentration for each cytokine in cell supernatants was determined by interpolation from the corresponding standard curve.

Determination of mouse CCL1 and CCL5 concentration. Concentration of mouse CCL1 and CCL5 from colons were determined by ELISA according to the manufacturers' instructions (R&D Systems).

Immunofluorescent staining of colon sections. Colon specimens were placed in Tissue-Tek optimum cutting temperature compound (Sakura), 'snap-frozen' in dry ice and ethanol and stored at –80 °C. Cryostat sections (10 μm in thickness) were affixed to Superfrost/Plus (Fisher Scientific) microscope slides, dried at 20–25 °C, fixed in cold acetone for 10 min and then dried at room temperature. Samples were rehydrated in Tris-buffered saline (TBS), pH 7.6, and then were blocked with 1% BSA and 5% NGS in TBS at room temperature for 1 to 2 h. Samples were then incubated at room

temperature for 1 to 2 h with R-PE-conjugated mouse F4/80-specific antibody (Serotec), FITC-conjugated mouse GR1-specific antibody (BD Pharmingen), or R-PE-conjugated mouse GR1-specific antibody (BD Pharmingen). After incubation with Hoechst 33342 (1 μg ml^{-1}, Dojindo) in TBS for 30 min to stain nuclei, samples were mounted in aqueous mounting medium, PERMAFLUOR (Beckman). The fluorescence images were acquired with a confocal laser-scanning microscope using the 405-nm line of an laser diode for excitation and a 430-nm to 460-nm band-pass filter for emission (Hoechst 33342), the 488-nm line of an argon laser for excitation and a 505-nm to 525-nm band-pass filter for emission (FITC), or the 543-nm line of a HeNe laser for excitation and a 560-nm long-pass filter for emission (PE). Numbers of GR1-positive neutrophils and F4/80-positive macrophages were counted in the images. The area occupied by GR1-positive neutrophils and F4/80-positive macrophages was quantified by Photoshop (Adobe)-based image analysis, and the number of neutrophils or macrophages per 200 × 200 μm^2 was calculated. In **Supplementary Fig. 6d**, the specimens were viewed at high magnification using plan oil objectives (× 60, 1.40 numerical aperture (NA), Olympus).

MPO assay. MPO activity was assessed essentially as previously described[8]. Colon specimens were homogenized in 0.5% hexadecyltrimethylammonium bromide in 50 mM phosphate buffer (pH 6.0) and sonicated for 10 s. Suspensions were freeze-thawed three times, and then centrifuged at 15,000 rpm for 15 min. One hundred μl of supernatant was mixed with a solution of 0.167 mg ml^{-1} *O*-dianisidine hydrochloride and 0.0005% hydrogen peroxide. MPO activity was measured spectrophotometrically as the change in absorbance at 460 nm.

cDNA and plasmids for retroviral infection. Mouse TRPM2 and mouse CXCL2 were subcloned into the pMXΔ retroviral vector[9].

Primary bone marrow cell culture and transduction. Bone marrow-derived macrophages (BMDMs) were prepared as described previously[10]. Briefly, nonadherent bone marrow cells of WT or *Trpm2* KO mice were cultured in RPMI 1640 containing 10% FBS, 0.1 mM nonessential amino acids, 2 mM L-glutamine, 100 units ml^{-1} penicillin, 100 μg ml^{-1} streptomycin, 1 mM sodium pyruvate, 50 mM 2-mercaptoethanol, and 20 ng ml^{-1} mouse M-CSF (PeproTech) for a total of 6–7 days. Adherent cells were >98% macrophages as judged by morphology and flow cytometer ($F4/80^{+}$).

Mouse TRPM2 or mouse CXCL2 was transduced into BMDMs by retroviral gene transfer at day 4 or 5 after isolation from the bone marrow. Briefly, TRPM2- or CXCL2-encoding retroviruses were produced by transfection of GP2-293 cells (Clontech) with retroviral constructs along with vesicular stomatitis virus G glycoprotein expression according to the manufacturer's protocol. Viral supernatants were collected 48 h after transfection, and added to BMDMs. After 48 h, the infection efficiency was assessed by measuring GFP fluorescence with flow cytometer, and the cells (infection efficiency: 40–50%) were used for experiments.

Transfer of BMDMs. BMDMs (5×10^6 cells in 500 μl of PBS) were injected into the tail vein of the mice administered with 2.5% DSS for 6 days. Twenty-four h later, colons were collected and utilized for immunostaining and MPO assay. Migration of

BMDMs into the colon was conformed by observing fluorophore-labeled BMDMs.

Histological evaluation of colonic lesions. The histological score of ulceration was calculated as previously described[11]. Rings of the transverse part of the proximal, middle, and distal colon were fixed in 10% formalin and embedded in paraffin, and each section was then stained with haematoxylin and eosin for the morphological evaluation. The histopathological change was graded on a scale from 0 to 3 according to the following criteria: 0, no remarkable change; 1, slight; 2, moderate; 3, marked. The histological score of ulceration was calculated by adding each score for proximal, middle, and distal colon.

Isolation of infiltrated cells into colon. The colon pieces were washed with RPMI 1640, then mechanically minced and resuspended in RPMI 1640 containing 2% FBS, antibiotics (30 units ml^{-1} penicillin and 30 mg ml^{-1} streptomycin), and 2,500 units ml^{-1} collagenase type IV (Worthington) for 30 min at 37 °C in a shaking incubator. After filtration of digested tissue with 70 μm nylon mesh, and washed with RPMI 1640. Isolated cells were analyzed by flow cytometer.

Flow cytometry. Cell suspensions were prepared from peripheral blood, bone marrow, and colon in RPMI 1640 containing 2% FBS and antibiotics (30 units ml^{-1} penicillin and 30 mg ml^{-1} streptomycin), then were washed and kept on ice. For flow cytometry, cells were plated at a density of about 1×10^6 cells per well in 96-well U-bottomed plates (Falcon), were stained for 30 min on ice with antibodies in 30 μl of PBS containing 2% FBS, 1 mM EDTA and 0.1% NaN_3, and then were washed with 200 μl of

this buffer. The following antibodies were used: FITC-conjugated mouse GR1-specific antibody, FITC-conjugated mouse CD11c-specific antibody (eBioscience), FITC-conjugated mouse NK1.1-specific antibody (eBioscience), FITC-conjugated mouse CD8a-specific antibody (eBioscience), PE-conjugated mouse CD8a-specific antibody (eBioscience), FITC-conjugated mouse CD4-specific antibody (eBioscience), PE-conjugated mouse CD4-specific antibody (eBioscience), PE-conjugated mouse F4/80-specific antibody (eBioscience), FITC-conjugated mouse Ly6C-specific antibody (BD Pharmingen), PE-conjugated mouse Ly6G-specific antibody (BD Pharmingen) and APC-conjugated mouse CD11b-specific antibody (BD Pharmingen). Data were collected on an EPICS Altra flow cytometer (Beckman Coulter) and were analyzed with EXPO32 software (Beckman Coulter).

CMTMR-labeled bone marrow cell injection. Bone marrow cells from femurs and tibias of WT or *Trpm2* KO mice were labeled with 20 μM 5- and 6-(4-chloromethyl)benzoyl-amino-tetramethylrhodamine (CMTMR) (Molecular Probes) for 30 min at 37 °C. After labeling, cells were washed extensively in RPMI 1640 supplemented with 2% FBS. CMTMR-labeled bone marrow cells were transferred by intravenous injection into the tail veins of WT mice administered with 2.5% DSS for 7 days. Next day, the colon was collected and CMTMR-labeled immunocytes were quantified by flow cytometer.

Neutrophil migration induced by intraperitoneal injection of CXCL2, CCL1, CCL3, CCL5, and fMLP. CXCL2 (1.0 μg), CCL1 (2.5 μg), CCL3 (1.0 μg), CCL5 (2.5 μg), and fMLP (10 nmol) in 500 μl PBS or PBS as control was intraperitoneally

injected into WT and *Trpm2* KO mice. After 30 min, peritoneal cells were obtained by lavage of the peritoneal cavity with 4 mL of sterile PBS. The number of neutrophils in peritoneal cells was quantified by flow cytometer. The number of migrated neutrophils was determined by subtracting neutrophil number in PBS-treated mice from that in chemoattractant-treated mice.

Measurement of body weight and colon length. Body weight was monitored throughout the experiment. Weight change was calculated as percent change in weight compared with day 0. Following eight days of 2.5% DSS administration, mice were performed euthanasia. The entire colon was extirpated, and the colon length was measured.

References

1. Hara, Y. *et al.* LTRPC2 Ca^{2+}-permeable channel activated by changes in redox status confers susceptibility to cell death. *Mol. Cell* **9**, 163–173 (2002).
2. Oh-hora, M., Johmura, S., Hashimoto, A., Hikida, M. & Kurosaki, T. Requirement for Ras guanine nucleotide releasing protein 3 in coupling phospholipase C-γ2 to Ras in B cell receptor signaling. *J. Exp. Med.* **198**, 1841–1851 (2003).
3. Lev, S. *et al.* Protein tyrosine kinase PYK2 involved in Ca^{2+}-induced regulation of ion channel and MAP kinase functions. *Nature* **376**, 737–745 (1995).
4. Yoshida, T. *et al.* Nitric oxide activates TRP channels by cysteine S-nitrosylation. *Nat. Chem. Biol.* **2**, 596–607 (2006).
5. Takeshima, H., Komazaki, S., Nishi, M., Iino, M. & Kangawa, K. Junctophilins: a novel family of junctional membrane complex proteins. *Mol. Cell* **6**, 11–22 (2000).

6. Nadler, M.J.S. *et al.* LTRPC7 is a Mg·ATP-regulated divalent cation channel required for cell viability. *Nature* **411**, 590–595 (2001).

7. Vig, M. *et al.* CRACM1 is a plasma membrane protein essential for store-operated Ca^{2+} entry. *Science* **321**, 1220–1223 (2006).

8. Han, X.B., Liu, X., Hsueh, W. & De Plaen, I.G. Macrophage inflammatory protein-2 mediates the bowel injury induced by platelet-activating factor. *Am. J. Physiol. Gastrointest. Liver Physiol.* **287**, G1220–G1226 (2004).

9. Mori, Y. *et al.* Transient receptor potential 1 regulates capacitative Ca^{2+} entry and Ca^{2+} release from endoplasmic reticulum in B lymphocytes. *J. Exp. Med.* **195**, 673–681 (2002).

10. Gough, P.J. *et al.* A disintegrin and metalloproteinase 10-mediated cleavage and shedding regulates the cell surface expression of CXC chemokine ligand 16. *J. Immunol.* **172**, 3678–3685 (2004).

11. Arai, Y., Takanashi, H., Kitagawa, H., Wirth, K.J. & Okayasu, I. Effect of icatibant, a bradykinin B2 receptor antagonist, on the development of experimental ulcerative colitis in mice. *Dig. Dis. Sci.* **44**, 845–851 (1999).